Polar-solvation classical density-functional theory for electrolyte aqueous solutions near a wall

Vadim Warshavsky and Marcelo Marucho

A Polar Solvation Classical Density Functional Theory Study on Electrolyte Aqueous Solutions Near a Wall

Vadim Warshavsky and Marcelo Marucho*

Department of Physics and Astronomy,

The University of Texas at San Antonio, San Antonio TX 78249-5003

A precise description of the structural and dielectric properties of liquid water is critical to understanding the physicochemical properties of solutes in electrolyte solutions. In this article, a mixture of ionic and dipolar hard spheres is considered to account for water crowding and polarization effects on ionic electrical double layers near a uniformly charged hard wall. As a unique feature, solvent hard spheres carrying a dipole at their centers were used to model water molecules at experimentally known concentration, molecule size and dipolar moment. The equilibrium ionic and dipole density profiles of this electrolyte aqueous model were calculated using a Polar Solvation Classical Density Functional Theory (PSCDFT). These profiles were used to calculate the charge density distribution, water polarization, dielectric permittivity function and mean electric potential profiles as well as differential capacitance, excess adsorptions and wall-fluid surface tension. These results were compared with those corresponding to the pure dipolar model and unpolar primitive solvent model of electrolyte aqueous solutions to understand the role that water crowding and polarization effects play on the structural and thermodynamic properties of these systems. Overall, PSCDFT predictions are in agreement with available experimental data.

I. INTRODUCTION

Electrolyte aqueous solutions play an important role in many technological, chemical, environmental and biological processes [1]. The importance of understanding the

---
*Electronic address: marcelo.marucho@utsa.edu

electrolyte solution effects on the electrical double layer (EDL) properties of solutes is reflected by the massive amount of works devoted to developing theoretical methods to predict their structural and thermodynamics properties. Signicant effort has been specially done to model nano-sensors and nano-adsorbents for sensing and removal of low concentrations of heavy toxic (mercury) ions in water under drinking conditions [2]. Other works have been focussed in modeling cell membranes interacting with low concentrations of sodium, potassium and chloride ions (generally found in gastric and pancreatic juices, bile and sweat) for diagnosing and treating biological electrolyte disorders [3]. These kind of studies on solutes interacting with liquids at low electrolyte concentrations have gained increased attention recently and are the target applications of the current work.

Among the broad theoretical approaches proposed to study these systems, the most used methods are those of numerical experiments, integral equations theory, Poisson-Boltzmann theory, classical and electronic Density Functional Theory (DFT) and a combination of these methods [4]. The major advantages of the classical DFT (compared to the 'exact' methods of the numerical experiment) are the low computational cost and good accuracy, which depend on the electrolyte model and approximate approach used to perform the calculations. Additionally, the equations of DFT establishes 'bridges' between the macroscopic thermodynamics and the microscopic molecular description. More importantly, the defiance of classical DFT is that it can be primarily used with the most simple intermolecular potential models and approximations and, therefore, it is the theoretical framework used in the present article.

The most simple electrolyte model treats ions as point-like charges whereas the solvent is modelled as a dielectric medium with permanent dielectric permittivity. This electrolyte model only accounts for the electrostatics, omitting any steric particle-particle interaction and solvent polarization. More sophisticated electrolyte models such as the Primitive Model (PM) and its modified versions also consider ion-ion exclude volume interactions, but they still neglect important solvent effects on EDLs. A more accurate approach to these implicit solvent models is given by the Solvent Primitive Model (SPM), which additionally accounts for crowding solvent effects. While this explicit solvent model considers solvent molecules as neutral hard spheres, it is unable to capture the dielectric inhomogeneities arising from the dipolar solvent orientation and ion- solvent dipole inter-

actions. In highly polar liquids like water these inhomogeneities are more pronounced, having a high bulk dielectric permittivity constant (compared to other liquids) that weakens the coulombic attractive forces between oppositely charged particles. This is because a significant part of the interaction energy is spent aligning so many intervening strong water dipoles. Additionally, the high water concentration is responsible for the strong ionic layering formation [24, 25, 70]. Consequently, modeling water molecules at experimentally known concentration, molecule size and dipolar moment is a prerequisite to accurately describe these phenomena. The simplest electrolyte solution model that treats ions and dipolar solvent molecules on the same theoretical footing is the ('civilized') Ion-Dipole Model (IDM), where solvent molecules are represented by hard spheres carrying a dipole at their centers. This model makes possible the detailed description of microscopic electrostatic interactions between solute ions and solvent molecules [5–10]. Accordingly, a refined ion-dipole electrolyte aqueous solution model is considered in this article to account for water crowding and polarization effects on the ionic electrical double layers near a uniformly charged hard wall.

Along with the aforementioned electrolyte solution models, several approximate approaches were proposed within classical DFT formalism to capture solvent polarization and crowding contributions to the potential of mean force of the system. The Poisson Boltzmann (PB) equation [11] as well as the Mean Spherical Approximation (MSA) for unpolar charged particle fluids [12, 13] and its modified versions [14, 15] were implemented to estimate the pure and residual electrostatic part of the potential of mean force, respectively. Moreover, the Weighted Density Approximation (WDA) [16] and, subsequently, the most powerful Fundamental Measure Theory (FMT) [17] and its modified versions [18–20] were developed to estimate the corresponding hard-sphere contributions to the potential of mean force. For instance, PB/MSA/WDA -DFT was used to study the ionic atmosphere near a planar wall [21–23], whereas PB/MSA/FMT -DFT was employed to investigate the ionic atmosphere outside spherical macroions [24], outside cylindrical DNA biomolecules [25], and near a planar wall [26]. One of the main advantages of FMT-DFT over WDA-DFT is that FMT-DFT is able to accurately describe hard sphere liquids at high concentration including those representing solvent molecules. In particular, the so-called White Bear II (WBII) version of FMT [20, 33] has been shown to be accurate in describing inhomogeneous fluids, mainly near solid subtracts [24, 25] and, therefore, it is

the approach considered in this article to calculate the pure HS contributions to the structural and thermodynamical properties of the ionic electrical double layers near a uniformly charged hard wall.

Other approaches were proposed within the DFT framework to study thermodynamic and structural features of pure polar fluids. While the Mean Field Approximation (MFA) and the so-called Modified Mean Field Approximation (MMFA) [34–45] for pair correlation functions of polar fluids are the most simple models capable of revealing the dipolar ordering in the electric field, they predict small values of the dielectric permittivity ε, which are typically given by a Clausius-Mosotti formula. An alternative approach to approximate interparticle correlations of dipole molecules was proposed by Wertheim [46], who obtained analytic expressions of the MSA for the angle-dependent Direct Correlation Function (DCF) of pure HS dipole fluids. This approach was used to calculate the polarization of dipolar fluids near a wall [47, 48] and a spherical macroion [48]. One of the advantages of MSA over MFA and MMFA is that the former is able to describe dipolar fluids with large dielectric permittivity ε, including that of water, although the accuracy of this approximation depends on the strength of the dipole moment. Other sophisticated models such as the IDM were used within MSA-DFT formalism to study electrolyte aqueous solutions [51, 52]. Blum and co-workers calculated in analytic form the MSA-DCF of the IDM for symmetric particle sizes [53–55], which certainly improves the oversimplified mean-field description of the correlations in ion-dipole mixture fluids. MSA-DCF still lacks some information on dipole correlations due to the linear dependence of the dipole-dipole part of MSA-DCF on the dipolar moment strength. Nevertheless, this approach is able to predict the experimental value of the water bulk dielectric constant when water molecules are represented at realistic values of size, density and dipolar moment. Accordingly, MSA-DCF is considered in this article to account for the dielectric inhomogeities appearing in the electrical double layers near a uniformly charged hard wall.

Certainly, the previous analysis points out the importance of developing more accurate and efficient approaches to provide a better understanding on the structural, thermodinamic as well as dielectrical properties of EDLs. In pursuit of this challenge, we introduce in this article a Polar Solvation Classical Density Functional Theory (PSCDFT) to calculate the equilibrium ionic and dipole density profiles of a refined ion-dipole electrolyte aqueous solution model. This is a straightforward extension of the Unpolar Solva-

tion Classical Functional Density Functional Theory (USCDFT) recently introduced by M. Marucho and collaborators [24, 25] to describe symmetric solutes immersed in unpolar electrolyte aqueous solutions. USCDFT predictions on spherical and cylindrical solutes were validated numerically and experimentally. It uses the SPM as well as the PB equation, the MSA, and the FMT-WBII approximations within the DFT formalism. In the present approach, the SPM is replaced by the IDM to study water polarization and crowding effects on the electrical and structural properties of electrolyte aqueous solutions near a uniformly charged planar surface. The resulting novel coupling between these approximations takes advantage of the accuracy of the FMT-WBII to estimate the correlations in the hard sphere model. It employs the simplicity of MSA-DCF [53–55] to estimate the residual electrostatic charge-charge, charge-dipole and dipole-dipole correlations. It also exploits the efficiency of the PB equation to calculate the mean electrostatic potential of the system. When compared with USCDFT, the proposed computational model incorporates important dielectric properties of electrolyte aqueous solutions near charged walls without increasing significantly the computational cost. Thus, PSCDFT becomes an extremely useful tool when a good balance between accuracy and efficiency in predicting structural and dielectric properties of EDLs is highly desired. This is crucial for studying those properties requiring repeated calculations of density profiles under multiple electrolyte aqueous solutions and physicochemical properties of solutes. PSCDFT was used to study the effects of water concentration and dipolar moment, electrolyte concentration, and wall surface charge density on the ionic layering formation, polarization, dielectric function and mean electric potential profiles. Relevant thermodynamic properties of the system such as differential capacitance, excess adsorptions and wall-fluid surface tension were also analyzed.

The rest of the paper is organized as follows. PSCDFT is described in Section II whereas the results obtained for the pure HS dipolar model, the unpolar primitive solvent model and IDM of electrolyte solutions near a charged wall are presented and analyzed in Section III. Section IV contains the summary, and the details of calculations are presented in Appendix.

II. DENSITY FUNCTIONAL THEORY FOR ION-DIPOLE FLUIDS

We consider a three-component molecular fluid that consists of a mixture of hard spheres carrying electric charges $q_i = \xi_i|e|$ ($i = 1, 2$, $|\xi_i|$ is valency, e an electron charge) and hard sphere solvent particles with electric dipole moment $\vec{m}$ located at the centers. For simplicity and computational efficiency, all the particles in the systems have the same diameter d. The ion-ion u_{ij}, ion-dipole u_{id} and dipole-dipole u_{dd} potentials of interaction between the particles in the mixture outside the hard-core ($r_{12} \geq d$) are given by the following expressions

$$u_{ij}(\vec{r}_1, \vec{r}_2) = \frac{q_i q_j}{r_{12}}, \tag{1}$$

$$u_{id}(\vec{r}_1, \vec{r}_2, \omega_2) = \frac{q_i m}{r_{12}^2} \Phi^{(011)}(\hat{r}_{12}, \hat{m}_2), \tag{2}$$

$$u_{dd}(\vec{r}_1, \omega_1, \vec{r}_2, \omega_2) = -\frac{m^2}{r_{12}^5} \Phi^{(112)}(\hat{r}_{12}, \hat{m}_1, \hat{m}_2), \tag{3}$$

where $\vec{r}_1$ and $\vec{r}_2$ denote the center positions of two molecules and $r_{12} = |\vec{r}_{12}| = |\vec{r}_2 - \vec{r}_1|$ is the corresponding intermolecular distance. Inside the hard-core ($r_{12} < d$) the potentials u_{ij}, u_{id} and u_{dd} are infinity. The orientation of a dipole moment $\vec{m}_k$ at the point $\vec{r}_k$ ($k = 1, 2$) is characterized by a body angle $\omega_k = (\theta_k, \varphi_k)$,. The angular functions $\Phi^{(011)}$ and $\Phi^{(112)}$ are represented by rotational invariants [56]

$$\Phi^{(011)}(\hat{r}_{12}, \hat{m}_2) = (\hat{r}_{12} \cdot \hat{m}_2),$$
$$\Phi^{(112)}(\hat{r}_{12}, \hat{m}_1, \hat{m}_2) = 3(\hat{m}_1 \cdot \hat{r}_{12})(\hat{m}_2 \cdot \hat{r}_{12}) - (\hat{m}_1 \cdot \hat{m}_2), \tag{4}$$

where $\hat{r}_{12}$, $\hat{m}_1$ and $\hat{m}_2$ are unit vectors along $\vec{r}_{12}$, $\vec{m}_1$ and $\vec{m}_2$ directions, respectively.

We consider an electrolyte solution near a planar charged electrode plate in a slab-shaped infinite system with the xy plane oriented parallel to the electrode plate. The wall is located at $z = z_0$ and the electrolyte occupies the part of the space $z \geq z_0$. The potential of interaction between the hard-spheres and hard wall is $V_{hw}^{(ext)}(z) = \infty$ for $z < z_0 + d/2$ and $V_{hw}^{(ext)}(z) = 0$ for $z \geq z_0 + d/2$.

We denote $\rho_i(\vec{r})$ ($i = 1, 2$) the local number density of ions of type i at position $\vec{r}$ and $\rho_d(\vec{r}, \omega)$ the one of dipoles

$$\rho_d(\vec{r}, \omega) = \rho_3(\vec{r})(\frac{1}{4\pi} + \alpha(\vec{r}, \omega)), \tag{5}$$

where $\alpha(\vec{r}, \omega)$ represents the distribution function of the molecular orientation ω with normalization

$$\int d\omega \alpha(\vec{r}, \omega) = 0, \tag{6}$$

and $\rho_3(\vec{r})$ is the angular average number density of dipoles

$$\int d\omega \rho_d(\vec{r}, \omega) = \rho_3(\vec{r}). \tag{7}$$

The equations of DFT and the expression for the grand canonical potential of a single component system in an external field can be found in Refs. [57–59]. We provide a brief summary of this formulation in Appendix A. Below we generalize this theory to the case of the ion-dipole mixture.

Based on the equation (A2) the grand canonical density functional can be expressed as

$$\Omega[\rho_i, \rho_d] = \Omega_{bulk}[\rho_{i,b}] + \Delta\Omega[\rho_i, \rho_d]. \tag{8}$$

Here, the short notation $[\rho_i, \rho_d]$ stands for $[\rho_1(\vec{r}), \rho_2(\vec{r}), \rho_d(\vec{r}, \omega)]$. The grand canonical potential $\Omega_{bulk}[\rho_{i,b}]$ depends on the bulk densities. The short notation $[\rho_{i,b}]$ stands for $[\rho_{1,b}, \rho_{2,b}, \rho_{3,b}]$, where $\rho_{1,b} = \rho_{2,b} = \frac{\rho_{0,b}}{2}$ are the bulk ionic densities and $\rho_{3,b}$ the one for dipole species.

Similar to (A3)-(A6), the functional $\Delta\Omega[\rho_i, \rho_d]$ in the rhs of Eq.(8) can be expressed as

$$\Delta\Omega[\rho_i, \rho_d] = \Delta\Omega_{igas}[\rho_i, \rho_d] + \Delta\Omega_{ext}[\rho_i, \rho_d] + \Delta\Omega_{int}[\rho_i, \rho_d]. \tag{9}$$

Here the ideal-gas term $\Delta\Omega_{gas}[\rho_i, \rho_d]$ is given by

$$\Delta\Omega_{igas}[\rho_i, \rho_d] = k_B T \Sigma_{i=1}^2 \int d\vec{r}[\rho_i(\vec{r}) \ln(\frac{\rho_i(\vec{r})}{\rho_{i,b}}) - \rho_i(\vec{r}) + \rho_{i,b}] +$$
$$k_B T \int \int d\vec{r} d\omega [\rho_d(\vec{r}, \omega) \ln(\frac{\rho_d(\vec{r}, \omega)}{\rho_{3,b}}) - \rho_d(\vec{r}, \omega) + \rho_{3,b}]. \tag{10}$$

The contribution of the external field of the charged wall acting on the electrolyte solution $\Delta\Omega_{ext}[\rho_i, \rho_d]$ can be written as

$$\Delta\Omega_{ext}[\rho_i, \rho_d] = \sum_{i=1}^{3} \int d\vec{r}\, V_{hw}^{(ext)}(\vec{r})\rho_i(\vec{r}) + \sum_{i=1}^{2} \int d\vec{r}\, q_i\rho_i(\vec{r})\varphi^{(ext)}(\vec{r})$$

$$- \int d\vec{r}d\omega\, (\vec{m}\cdot\vec{E}^{(ext)}(\vec{r}))\rho_d(\vec{r},\omega), \tag{11}$$

where $\varphi^{(ext)}(\vec{r})$ is the external electric potential and $\vec{E}^{(ext)}(\vec{r})$ the external electric field. The contribution of the intrinsic interaction between molecules $\Delta\Omega_{int}[\rho_i, \rho_d]$ is given by

$$\Delta\Omega_{int}[\rho_i, \rho_d] = -\frac{1}{2\beta}\sum_{i,j=1}^{2} \int d\vec{r}d\vec{r'}\Delta\rho_i(\vec{r}_1)\Delta\rho_j(\vec{r}_2)c_{ij}^{(2)}(\vec{r}_1, \vec{r}_2)$$

$$-\frac{1}{\beta}\sum_{i=1}^{2} \int d\vec{r}_1 d\vec{r}_2 d\omega_2 \Delta\rho_i(\vec{r}_1)\Delta\rho_d(\vec{r}_2,\omega_2)c_{id}^{(2)}(\vec{r}_1, \vec{r}_2, \omega_2)$$

$$-\frac{1}{2\beta} \int d\vec{r}_1 d\vec{r}_2 d\omega_1 d\omega_2 \Delta\rho_d(\vec{r}_1,\omega_1)\Delta\rho_d(\vec{r}_2,\omega_2)c_{dd}^{(2)}(\vec{r}_1, \omega_1, \vec{r}_2, \omega_2), \tag{12}$$

where $c_{ij}^{(2)}$, $c_{id}^{(2)}$, and $c_{dd}^{(2)}$ denote the ion-ion, ion-dipole and dipole-dipole direct correlation functions, respectively. On the other hand, $\Delta\rho_i(\vec{r}) = \rho_i(\vec{r}) - \rho_{i,b}$ and $\Delta\rho_d(\vec{r},\omega) = \rho_d(\vec{r},\omega) - \frac{\rho_{3,b}}{4\pi}$ denote the wall perturbation on the bulk ion and dipole density distributions, respectively.

In the present study we use the Mean Spherical Approximation (MSA) to calculate the direct correlation functions $c_{ij}^{(2)}$, $c_{id}^{(2)}$ and $c_{dd}^{(2)}$. These functions can be expressed as a sum of short- and long-range parts, i.e.

$$c_{ij}^{(2)}(\vec{r}_1, \vec{r}_2) = c_{ij}^{(SR)}(\vec{r}_1, \vec{r}_2)\Theta(d - r_{12}) - \beta u_{ij}(\vec{r}_1, \vec{r}_2)\Theta(r_{12} - d),$$

$$c_{id}^{(2)}(\vec{r}_1, \vec{r}_2, \omega_2) = c_{id}^{(SR)}(\vec{r}_1, \vec{r}_2, \omega_2)\Theta(d - r_{12}) - \beta u_{id}(\vec{r}_1, \vec{r}_2, \omega_2)\Theta(r_{12} - d),$$

$$c_{dd}^{(2)}(\vec{r}_1, \omega_1, \vec{r}_2, \omega_2) = c_{dd}^{(SR)}(\vec{r}_1, \omega_1, \vec{r}_2, \omega_2)\Theta(d - r_{12}) - \beta u_{dd}(\vec{r}_1, \omega_1, \vec{r}_2, \omega_2)\Theta(r_{12} - d), \tag{13}$$

where the functions $c^{(SR)}\Theta(d - r_{12})$ account for the short-ranged correlations; $\Theta(x)$ is the Heaviside step-function: $\Theta(x) = 1$, for $x > 0$ and $\Theta(x) = 0$, for $x < 0$.

Extracting the hard-sphere part contribution $c^{(hs)}$ from the direct correlation function $c^{(SR)}$ in the rhs of Eqs. (13), the direct correlation functions $c^{(2)}$ can be expressed as

$$c_{ij}^{(2)}(\vec{r}_1, \omega_1, \vec{r}_2, \omega_2) = c_{ij}^{(hs)}(\vec{r}_1, \vec{r}_2)\Theta(d - r_{12}) - \beta u_{ij}(\vec{r}_1, \vec{r}_2)$$

$$+[c_{ij}(\vec{r}_1, \vec{r}_2) + \beta u_{ij}(\vec{r}_1, \vec{r}_2)]\Theta(d - r_{12}), \tag{14}$$

$$c_{id}^{(2)}(\vec{r}_1, \vec{r}_2, \omega_2) = c_{i3}^{(hs)}(\vec{r}_1, \vec{r}_2)\Theta(d - r_{12}) - \beta u_{id}(\vec{r}_1, \vec{r}_2, \omega_2)$$

$$+[c_{id}(\vec{r}_1, \vec{r}_2, \omega_2) + \beta u_{id}(\vec{r}_1, \vec{r}_2, \omega_2)]\Theta(d - r_{12}), \qquad (15)$$

$$c_{dd}^{(2)}(\vec{r}_1, \omega_1, \vec{r}_2, \omega_2) = c_{33}^{(hs)}(\vec{r}_1, \vec{r}_2)\Theta(d - r_{12}) - \beta u_{dd}(\vec{r}_1, \omega_1, \vec{r}_2, \omega_2)$$

$$+[c_{dd}(\vec{r}_1, \omega_1, \vec{r}_2, \omega_2) + \beta u_{dd}(\vec{r}_1, \omega_1, \vec{r}_2, \omega_2)]\Theta(d - r_{12}). \qquad (16)$$

The first terms in the rhs of Eqs.(14), (15), (16) $c_{ij}^{(hs)}\Theta(d - r_{12})$ are the short-ranged direct correlation functions of a pure hard-sphere fluid due to the hard-sphere repulsion. The second terms represent the ion-ion βu_{ij}, ion-dipole βu_{id}, dipole-dipole βu_{dd} correlations due to the electrostatic interaction between particles. In the same equations, the residual contributions $[c_{ij} + \beta u_{ij}]\Theta(d - r_{12})$, $[c_{id} + \beta u_{id}]\Theta(d - r_{12})$, and $[c_{dd} + \beta u_{dd}]\Theta(d - r_{12})$ can be interpreted as the results of mutual correlations between the electrostatic and hard-sphere interactions. The explicit expressions of the functions c_{ij}, c_{id}, and c_{dd} are given in Appendix B.

For convenience, we rearrange the contributions into Eq. (9) as follows

$$\Delta\Omega = \Sigma_{i=1}^3 \int d\vec{r} V_{hw}^{(ext)}(\vec{r})\rho_i(\vec{r}) + \Delta\Omega_{igas} + \Delta\Omega_{hs} + \Delta\Omega_{el} + \Delta\Omega_{res}. \qquad (17)$$

The first term in rhs of Eq.(17) is due to the hard-wall repulsion. The remaining terms in Eq.(17) are explained in detail below.

A. The ideal-gas contribution $\Delta\Omega_{igas}$

The second term in rhs of Eq.(17) is due to the ideal-gas contribution (see Eq.(10)). For orientational distribution $\alpha(\vec{r}, \omega)$ sufficiently small, i.e. $|\alpha(\vec{r}, \omega)| << 1$ we can expand the last contribution in rhs of Eq.(10) in powers of α up second order as follows

$$\Delta\Omega_{igas}[\rho_i, \rho_d] = \frac{1}{\beta}\Sigma_{i=1}^3 \int d\vec{r}[\rho_i(\vec{r})\ln(\frac{\rho_i(\vec{r})}{\rho_{i,b}}) - \rho_i(\vec{r}) + \rho_{i,b}] + \frac{2\pi}{\beta}\int\int d\vec{r}d\omega\rho_3(\vec{r})[\alpha(\vec{r}, \omega)]^2. \quad (18)$$

Clearly, the system under consideration is only inhomogeneous in z direction due to the translational invariant in the xy plane. Thus, the density profiles $\{\rho_i(z)\}$ and the

orientation distribution function $\alpha(z,\omega)$ depend on the spatial variable z only. Due to the same invariance the orientation distribution function $\alpha(z,\omega)$ is also independent on the axial angle ϕ. Thus, the function $\alpha(z,\omega)$ can be expressed in terms of the spherical harmonics $\{Y_{l0}(\omega)\}$ by

$$\alpha(z,\theta) = \sum_{l=1}^{\infty} \eta_{l0}(z) Y_{l0}(\omega). \tag{19}$$

Here the expansion coefficients $\{\eta_{lm}(\vec{r})\}$ play the role of the orientation order parameters where

$$\eta_{l0}(z) = \int d\omega \alpha(z,\omega) Y_{l0}^*(\omega). \tag{20}$$

Due to the presence of the external field, the free energy of homogeneous and inhomogeneous polar systems depend on the shape of the system [42, 60]. We first consider a system contained in a finite cylindrical volume V and then take the thermodynamical limit $V \to \infty$ such as the system adopts the slab shape. As a result, we can express $\Delta\Omega_{igas}$ as a functional of densities $\{\rho_i(z)\}$ and orientation order parameters $\{\eta_{l0}(z)\}$ profiles as follows

$$\lim_{V\to\infty} \Delta\Omega_{igas}[\rho_i,\eta_{l0}]/A = \lim_{L\to\infty} \frac{1}{\beta}\Sigma_{i=1}^3 \int_{z_0}^{L} dz[\rho_i(z)\ln(\frac{\rho_i(z)}{\rho_{i,b}}) - \rho_i(z) + \rho_{i,b}]$$
$$+ \frac{2\pi}{\beta}\int_{z_0}^{L} dz\rho_3(z)\sum_{l=1}^{\infty}[\eta_{l0}(z)]^2, \tag{21}$$

where A is the area of the system in $x-y$ direction. The short notation $[\rho_i,\eta_{l0}]$ stands for $[\rho_1(z),\rho_2(z),\rho_3(z),\eta_{l0}(z)]$. Hereafter we use the notation $\Delta\Omega_{igas}[\rho_i,\eta_{l0}]/A$ as the one in the thermodynamical limit, i.e. $\lim_{V\to\infty} \Delta\Omega_{igas}[\rho_i,\eta_{l0}]/A$ and the infinity notation ∞ in the upper boundary of integration instead of L (see Eqs.(25),(36)).

B.   The pure hard-sphere contribution $\Delta\Omega_{hs}[\rho_\alpha]$

The third term in rhs of Eq.(17) is due to the repulsive pure hard-sphere intermolecular interaction

$$\Delta\Omega_{hs} = -\frac{1}{2\beta}\sum_{i,j=1}^{3}\int d\vec{r_1}d\vec{r_2}\Delta\rho_i(\vec{r_1})\Delta\rho_j(\vec{r_2})c_{ij}^{(hs)}(\vec{r_1},\vec{r_2}). \tag{22}$$

To reduce rhs of Eq.(22) to a one-dimensional integration we use the path integration formula [57]

$$c_i^{(1)}([\rho_{i,\alpha}],\vec{r}_1) = c_i^{(1)}([\rho_{i,b}],\vec{r}_1) + \sum_{j=1}^{3}\int_0^\alpha d\alpha'\int d\vec{r}_2\Delta\rho_j(\vec{r}_2)c_{ij}^{(2)}([\rho_{i,\alpha'}];\vec{r}_1,\vec{r}_2), \qquad (23)$$

where $c_i^{(1)}([\rho_{i,\alpha'}],\vec{r}_1)$ is the one-particle direct correlation function evaluated at density $\rho_{i,\alpha'}(\vec{r}_1) = \rho_{i,b} + \alpha'\Delta\rho_i(\vec{r}_2)$.

To work out the Eq.(23) we approximate the two-particle direct correlation function $c_{ij}^{(2)}$ in the integrand in rhs of Eq.(23) by the one given for the bulk fluid (see Eq.(A8)). As a result, the Eq.(23) for HS system in the final inhomogeneous state with $\alpha = 1$ yields

$$-\frac{\delta\beta F_{hs}^{(ex)}[\rho_i]}{\delta\rho_i(\vec{r}_1)} = -\beta\mu_{hs,i}^{(ex)}[\rho_{i,b}] + \sum_{j=1}^{3}\int d\vec{r}_2\Delta\rho_j(\vec{r}_2)c_{ij}^{(hs)}([\rho_{i,b}];r_{12}) \qquad (24)$$

where $c_i^{(1)}[\rho_i] = -\delta\beta F^{(ex)}[\rho_i]/\delta\rho_i(\vec{r}_1)$, $c_i^{(1)}[\rho_{i,b}] = -\mu_{i,b}^{(ex)}[\rho_{i,b}]$ and $\mu_{i,b}^{(ex)}$ is the excess (over ideal-gas) chemical potential of the i-species in the bulk. Finally, the substitution of Eq.(24) into Eq.(22) produces the following result

$$\Delta\Omega_{hs}/A = -\frac{1}{2\beta}\sum_{i=1}^{3}\int_{z_0}^\infty dz\Delta\rho_i(z)(\beta\mu_{hs,i}^{(ex)}[\rho_{i,b}] - \frac{\delta\beta F_{hs}^{(ex)}[\rho_i]}{\delta\rho_i(z)}). \qquad (25)$$

In our proposal we estimate the excess HS free energy density functional $F_{hs}^{(ex)}$ using the Fundamental Measure (FM) theory, which is based on the geometrical properties of HS [17] (for recent reviews see [28, 61]). In the framework of FM-DFT, the excess free energy density $\Phi(\{n_\alpha(\vec{r})\})$ is expressed via a set of weighted densities $\{n_\alpha(\vec{r})\}$, each of them is a convolution of number density $\{\rho_i(\vec{r})\}$ with weight functions $\{\omega_\alpha^{(i)}\}$. The particular form of functional dependence of weighted densities $n_\alpha(z)$ on number densities $\rho_i(z)$ in Cartesian coordinates can be found in Refs. [18, 28]. In the present study we employ the so-called White Bear II density functional [20, 33]. Furthermore, we assume that the difference between Percus Yevick (MSA) and FM-WBII DFT approximations for HS direct correlation function $c_{ij}^{(hs)}$

$$\sum_{j=1}^{3}\int d\vec{r}_2\Delta\rho_j(\vec{r}_2)[c_{ij}^{(hs,MSA)}([\rho_{i,b}];r_{12}) - c_{ij}^{(hs,FMWBII)}([\rho_{i,b}];r_{12})] \quad (i=1,2,3)$$

is negligible compared to the corresponding contributions coming from the electrostatic correlations. Therefore, the residual contributions to the direct correlation function are still approximated within MSA. This mixing version of FM DFT, which reproduces the accurate HS Carnahan Starling equation of state and MSA DCFs for residual contributions, has been often used in the calculation of ionic fluids properties [24–26].

C. The pure electrostatic contribution $\Delta\Omega_{el}[\rho_i, \rho_d]$

The fourth term in rhs of Eq.(17) is due to the pure electrostatic interactions

$$\Delta\Omega_{el}[\rho_i, \rho_d] = \sum_{i=1}^{2} \int d\vec{r}\, q_i \rho_i(\vec{r}) \varphi^{(ext)}(\vec{r}) - \int d\vec{r} d\omega\, (\vec{m} \cdot \vec{E}^{(ext)}(r)) \rho_d(\vec{r}, \omega)$$

$$+ \frac{1}{2} \sum_{i,j=1}^{2} \int d\vec{r}_1 d\vec{r}_2 \Delta\rho_i(\vec{r}_1) \Delta\rho_j(\vec{r}_2) \frac{q_i q_j}{r_{12}}$$

$$+ \sum_{i=1}^{2} \int d\vec{r}_1 d\vec{r}_2 d\omega_2 \Delta\rho_i(\vec{r}_1) \Delta\rho_d(\vec{r}_2, \omega_2) \frac{q_i m}{r_{12}^2} \Phi^{(011)}(1,2)$$

$$- \frac{1}{2} \int d\vec{r}_1 d\vec{r}_2 d\omega_1 d\omega_2 \Delta\rho_d(\vec{r}_1, \omega_1) \Delta\rho_d(\vec{r}_2, \omega_2) \frac{m^2}{r_{12}^3} \Phi^{(112)}(\vec{r}_1, \omega_1, \vec{r}_2, \omega_2). \tag{26}$$

The electrostatic potential $\Delta\Omega_{el}$ in Eq.(26) can be written as a functional of the electric charge Q and polarization P density profiles as follows

$$\Delta\Omega_{el}[Q, P] = \int d\vec{r}\, Q(r) \varphi^{(ext)}(\vec{r}) - \int d\vec{r}\, (\vec{P}(r) \cdot \vec{E}^{(ext)}(\vec{r})) + \frac{1}{2} \int d\vec{r}\, Q(r) \varphi_Q(\vec{r}) +$$

$$\frac{1}{2} \int d\vec{r}\, Q(r) \varphi_P(\vec{r}) - \frac{1}{2} \int d\vec{r}\, (\vec{P}(r) \cdot \vec{E}_Q(\vec{r})) - \frac{1}{2} \int d\vec{r}\, (\vec{P}(r) \cdot \vec{E}_P(\vec{r})), \tag{27}$$

where

$$\varphi_Q(\vec{r}_2) = \int \frac{Q(\vec{r}_1)}{|\vec{r}_1 - \vec{r}_2|} d\vec{r}_1, \tag{28}$$

$$\varphi_P(\vec{r}_2) = \int \frac{(\vec{P}(\vec{r}_1) \cdot \hat{r}_{12})}{|\vec{r}_1 - \vec{r}_2|^2} d\vec{r}_1, \tag{29}$$

$$\vec{E}_Q(\vec{r}_2) = - \int \frac{Q(\vec{r}_1) \hat{r}_{12}}{|\vec{r}_1 - \vec{r}_2|^2} d\vec{r}_1, \tag{30}$$

$$\vec{E}_P(\vec{r}_2) = \int \frac{[3(\vec{P}(\vec{r}_1)\cdot\hat{r}_{12})\hat{r}_{12} - \vec{P}(\vec{r}_1)]}{|\vec{r}_1 - \vec{r}_2|^3} d\vec{r}_1, \tag{31}$$

$$Q(\vec{r}) = \sum_{i=1}^{2} q_i \rho_i(\vec{r}), \tag{32}$$

$$\vec{P}(\vec{r}) = \int \vec{m} \rho_d(\vec{r},\omega) d\omega. \tag{33}$$

Here $\varphi_Q(\vec{r}_1)$ is the electrostatic potential of ions, $\varphi_P(\vec{r})$ the electrostatic potential of dipoles, $\vec{E}_Q(\vec{r})$ the electric field induced by the ions, $\vec{E}_P(\vec{r})$ the electric field induced by the dipoles, and $Q(\vec{r})$ and $\vec{P}(\vec{r})$ the density profiles of the electric charge and polarization.

With help of Eqs.(5),(19) and with use of the symmetry of the system, Eqs.(32), (33) can be written as follows

$$Q(z) = \xi_1 e \rho_1(z) + \xi_2 e \rho_2(z), \tag{34}$$

$$P(z) = (\frac{4\pi}{3})^{\frac{1}{2}} m \rho_3(z) \eta_{10}(z). \tag{35}$$

Finally, substituting these expressions into Eq.(27), we can rewrite the functional $\Delta\Omega_{el}[Q, P]$ in the following form

$$\Delta\Omega_{el}[Q, P]/A = \frac{1}{2}\int_{z_0}^{\infty} dz Q(z)\varphi^{(ext)}(z) - \frac{1}{2}\int_{z_0}^{\infty} dz P(z)E^{(ext)}(z)$$
$$+\frac{1}{2}\int_{z_0}^{\infty} dz Q(z)\varphi(z) - \frac{1}{2}\int_{z_0}^{\infty} dz P(z)E(z), \tag{36}$$

where the combined electrostatic potential $\varphi(z)$ and the electric field $E(z)$ are introduced as

$$\varphi(z) = \varphi^{(ext)}(z) + \varphi_Q(z) + \varphi_P(z), \tag{37}$$

$$E(z) = E^{(ext)}(z) + E_Q(z) + E_P(z). \tag{38}$$

To express the electrostatic potential $\varphi(z)$ and the electric field $E(z)$ as functionals of the electric charge $Q(z)$ and the polarization $P(z)$ profiles in the obvious form we start with the electrostatic Maxwell equation [62]

$$-\frac{d^2\varphi(z)}{dz^2} = 4\pi Q(z) - 4\pi\frac{dP(z)}{dz}. \tag{39}$$

The latter can be transformed after two integrations of both parts of Eq.(39) with use of two boundary conditions $\varphi(z_0) = \varphi_0$ and $\varphi(\infty) = 0$ for two constants of integration and with use of the electroneutrality condition

$$\sigma = -\int_{z_0}^{\infty} dzQ(z), \tag{40}$$

where σ is a surface charge density. Thus, we have

$$\varphi(z) = \varphi_0 + 4\pi\int_{z_0}^{+\infty}(z'-z_0)Q(z')dz' + 4\pi\int_{z}^{\infty}(z-z')Q(z')dz' + 4\pi\int_{z_0}^{z}P(z')dz', \tag{41}$$

$$E(z) = -\frac{\partial\varphi(z)}{\partial z} = -4\pi\int_{z}^{\infty}Q(z')dz' - 4\pi P(z). \tag{42}$$

D.   The residual contribution $\Delta\Omega_{res}[\rho_i, \rho_d]$

The last term in rhs of Eq.(17) can be expressed as

$$\Delta\Omega_{res}[\rho_i, \rho_d] = -\frac{1}{2\beta}\sum_{i,j=1}^{2}\int d\vec{r}_1 d\vec{r}_2 \Delta\rho_i(\vec{r}_1)\Delta\rho_j(\vec{r}_2)[c_{ij}(\vec{r}_1, \vec{r}_2) + \beta u_{ij}(\vec{r}_1, \vec{r}_2)]\Theta(d - r_{12})$$

$$-\frac{1}{\beta}\sum_{i=1}^{2}\int d\vec{r}_1 d\vec{r}_2 d\omega_2 \Delta\rho_i(\vec{r}_1)\Delta\rho_d(\vec{r}_2, \omega_2)[c_{id}(\vec{r}_1, \vec{r}_2, \omega_2) + \beta u_{id}(\vec{r}_1, \vec{r}_2, \omega_2)]\Theta(d - r_{12})$$

$$-\frac{1}{2\beta}\int d\vec{r}_1 d\vec{r}_2 d\omega_1 d\omega_2 \Delta\rho_d(\vec{r}_1, \omega_1)\Delta\rho_d(\vec{r}_2, \omega_2)[c_{dd}(\vec{r}_1, \omega_1, \vec{r}_2, \omega_2)$$

$$+\beta u_{dd}(\vec{r}_1, \omega_1, \vec{r}_2, \omega_2)]\Theta(d - r_{12}). \tag{43}$$

After integrating the body angles ω_1, ω_2 and the volume $\vec{r}_2$ in the rhs of Eq. (43) the residual potential $\Delta\Omega_{res}$ can be written as a functional of the charge $Q(z)$ and the polarization $P(z)$ densities in suitable form for numerical computation as follows

$$\Delta\Omega_{res}[Q, P]/A = \frac{1}{2}\int_{z_0}^{+\infty} dz_1 Q(z_1)\varphi_{res}^{(qq)}(z_1)$$

$$+\frac{1}{2}\int_{z_0}^{+\infty}dz_1 Q(z_1)\varphi_{res}^{(qd)}(z_1)-\frac{1}{2}\int_{z_0}^{+\infty}dz_1 P(z_1)E_{res}^{(qd)}(z_1)$$

$$-\frac{1}{2}\int_{z_0}^{+\infty}dz_1 P(z_1)E_{res}^{(dd)}(z_1). \qquad (44)$$

The one dimensional integral expressions for the functions $\varphi_{res}^{(qq)}(z_1)$, $\varphi_{res}^{(qd)}(z_1)$, $E_{res}^{(dq)}(z_1)$ and $E_{res}^{(dd)}(z_1)$ are given in Appendix C.

E.   Master equations and computational scheme

The density and order parameter profiles are determined by the variational principle

$$\frac{\delta\Omega[\rho_i,\eta_{l0}]}{\delta\rho_i(z)}=0,\quad (i=1,2,3)\qquad\frac{\delta\Omega[\rho_i,\eta_{l0}]}{\delta\eta_{l0}(z)}=0\quad (l=1,...)\qquad(45)$$

From Eqs.(45) with help of Eqs.(22), (24),(34),(35),(37), (38),(C6),(C7),(47),(48) the density profiles $\{\rho_i(z)\}$ and $\eta_{10}(z)$ can be found as the numerical solution of the set of coupled integral equations

$$\begin{cases} \rho_i(z)=\rho_{i,b}\,\exp\{\beta\mu_{hs,i}^{(ex)}-\frac{\delta F_{hs}^{(ex)}}{\delta\rho_i(z)}-\beta V_i^{(wall)}-\beta z_i e\tilde{\varphi}(z)\}, & (i=1,2)\\[3mm] \rho_3(z)=\rho_{3,b}\,\exp\{\beta\mu_{hs,3}^{(ex)}-\frac{\delta F_{hs}^{(ex)}}{\delta\rho_3(z)}-\beta V_3^{(wall)}+(\frac{\pi}{3})^{\frac{1}{2}}\beta m\eta_{10}(z)\tilde{E}(z)\}, & (46)\\[3mm] \eta_{10}(z)=\frac{1}{2}(\frac{1}{3\pi})^{\frac{1}{2}}\beta m\tilde{E}(z), \end{cases}$$

where the total electrostatic potential $\tilde{\varphi}(z_1)$ and the electric field $\tilde{E}(z_1)$ are defined as

$$\tilde{\varphi}(z)=\varphi(z)+\varphi_{res}^{(qq)}(z)+\varphi_{res}^{(qd)}(z), \qquad (47)$$

$$\tilde{E}(z)=E(z)+E_{res}^{(qd)}(z)+E_{res}^{(dd)}(z). \qquad (48)$$

Due to the MSA approximations, the orientation order parameters $\eta_{l0}(z)$ are equal to zero for $l>1$. Note that the last equation in Eqs.(46) can be rewritten, with help of Eq.(35), as follows

$$P(z)=<m>\rho_3(z). \qquad (49)$$

where $<m>=\frac{\beta m^2}{3}\tilde{E}(z)$ is an average dipole moment and the value $\frac{\beta m^2}{3}$ is the orientational polarization of the particle.

We use the following Picard-like iterative algorithm to solve the set of integral equations (46)

$$
\begin{cases}
\rho_{i,in}^{(k+1)} = \rho_{i,out}^{(k)} = \hat{A}_i[\{\rho_{\alpha,in}^{(k)}\}, \eta_{10,in}^{(k)}], & (i = 1, 2, 3) \\
\\
\eta_{10,in}^{(k+1)} = \eta_{10,out}^{(k)} = \hat{A}_4[\{\rho_{i,in}^{(k)}\}, \eta_{10,in}^{(k)}]
\end{cases}
\tag{50}
$$

where $\hat{A}_i$ (i=1,2,3) and $\hat{A}_4$ are the integral operators in the right-hand sides of the set of four integral equations (46). We used the following mixing scheme to improve the convergence and avoid instabilities in the iterations

$$
\begin{cases}
\rho_{i,in}^{(k+1)} = \kappa \rho_{i,out}^{(k)} + (1 - \kappa)\rho_{i,in}^{(k)}, & (i = 1, 2, 3) \\
\\
\eta_{10,in}^{(k+1)} = \kappa \eta_{10,out}^{(k)} + (1 - \kappa)\eta_{10,in}^{(k)}
\end{cases}
\tag{51}
$$

where the mixing parameter κ ranges from 0.01 to 0 0.001 depending on the ionic bulk densities. The iteration is over when the residual tolerance between two consecutive iterations is less than eight digits of precision. The average CPU time to run the PSCDFT code in one processor is around 15 minutes, which is approximately 3 times longer than running the corresponding USCDFT code. Thus, the use of the proposed polarization model does not increase significantly the typical computational cost obtained for unpolar electrolyte solutions.

The surface charge density σ and the electrostatic potential φ_0 of the electrode plate are parameters of the calculations. They are not independent of each other. For the mere purpose of numerical convergence we chose the potential φ_0 as an input parameter, whereas the surface charge density σ is calculated from the charge neutrality condition in Eq.(40).

Once the profiles of the densities and orientational order parameter are obtained the thermodynamic characteristics of the electrical double layer can be calculated. The adsorption Γ_i of species $i(= 1, 2, 3)$ is defined as

$$
\Gamma_i = \int_{z_0}^{\infty} [\rho_i(z) - \rho_{i,b}]dz,
\tag{52}
$$

whereas the wall-fluid surface tension γ is calculated as follows

$$\gamma = \frac{\Omega(\mu, T) - \Omega_{bulk}(\mu, T)}{A}.$$ (53)

III.   RESULTS AND DISCUSSIONS

In this section, several electrolyte aqueous solutions and solute configurations were considered to analyze changes on the EDL properties of the system arising from changes on monvalent salt concentrations and wall charge densities. The results predicted by several electrolyte models were compared to understand the role that water crowding and polarization effects play on their structural and thermodynamic properties.

For numerical calculation purposes, the following dimensionless parameters were used: density $\rho^* = \rho d^3$, electric charge $q^* = (\frac{\beta}{d})^{\frac{1}{2}} q$, dipole moment $m^* = (\frac{\beta}{d^3})^{\frac{1}{2}} m$, electric field $E^* = (\beta d^3)^{\frac{1}{2}} E$, polarization $P^* = (\beta d^3)^{\frac{1}{2}} P$, electrostatic potential $\varphi^* = \beta e \varphi$, electric charge density $\sigma^* = \sigma(\beta d^3)^{\frac{1}{2}}$, excess adsorptions $\Gamma_i^* = \Gamma_i/(\rho_{i,b} d)$ (i=1,2,3), and surface tension $\gamma^* = \beta \gamma d^2$. For simplicity, the origin of the reference system ($z_0 = 0$) was chosen to be on the surface of the hard wall.

A.   Hard Sphere Dipoles near Planar Charged Surfaces

Hard spheres with molecular diameter $d = 2.75 \mathring{A}$ and weight density at room temperature $1 \, g/cm^3$ were used to describe the structural properties of liquid water. These values of the parameters yield dimensionless number density $\rho_b^* = 0.70$ and molar concentration $c = 55.35 M$. Additionally, a dipole moment $m = 2.22 \, D$ at the center of the hard spheres was used to describe the dielectric properties of liquid water. Note that this value of dipole moment is within the range of values used in many molecular water models in the liquid state [63]. More importantly, within the MSA-DCF formalism used in this work (see Ref.[46]), it leads to a dielectric permittivity constant $\varepsilon = 79.7$, which is in good agreement with the corresponding experimental value[64].

This liquid water model was used to calculate the orientational order parameter profile $\eta_{10}(z) = < \cos\theta >$ for different values of the wall charge density σ^*. This parameter provides useful information on the angular average anisotropic interactions between the

external electric field and the solvent dipolar moment (see Fig. 1). It takes absolute values ranging from zero, in the case when the dipole orientation is fully isotropic, to one when the dipoles are perfectly aligned. Fig. 1 shows that increased values of the wall charge density σ^* generates large oscillations of the order parameter $\eta_{10}(z)$ which widens the inhomogeneity of this profile near the wall. A high charge density σ^* also induces strong dipole ordering along the long-range wall electric field $E_0^* = 4\pi\sigma^*$ and, consequently, high bulk orientational order parameter.

On the other hand, the approach and model considered in this section are not able to capture the wall charge density effects on the water number density profiles. A different scenario is observed in the polarization profile $P(z)$, where increased charge density σ^* generates higher peaks, making more pronounced the inhomogeneity of these profiles near the wall. This is mainly due to the linear dependence between the polarization profile and the orientational order parameter $\eta_{10}(z)$ and the water number density $\rho(z)$ (see Eq. (35)). This phenomenon is depicted in Fig. 2 where the dimensionless electric polarization profiles $P^*(z)$ are represented for the same values of the charge densities σ^* used in Fig. 1. These results are critical to understanding the molecular mechanisms behind dielectric inhomogeneities arising in EDLs. For instance, the dielectric permittivity ε in the bulk solvent depends on the polarization P and the Maxwell electric field E as follows [65]

$$\varepsilon = 1 + 4\pi\frac{P}{E}. \tag{54}$$

Eq. (54) can be also used to estimate the dielectric permittivity profile $\varepsilon(z)$ in weakly inhomogeneous systems and small bulk dielectric permittivity ϵ (Clausius-Mosotty formula [38, 42, 51]). However, it cannot be applied in the current form for large dielectric permittivity and high inhomogeneity (see Fig. 2) as it is the case under consideration in the present work ([10, 66–69]). Several approaches [10] were proposed to extend the applicability of Eq. (54) to high bulk dielectric permittivities by smoothing the polarization profiles $P(z)$. However, these approaches are still not quite helpful for highly inhomogeneous systems. To overcome this shortcoming, Oleksy and Hansen [69] proposed a sigmoidal function which qualitatively describes inhomogeneous dielectric properties of polar fluids. Accordingly, the expression for the dielectric permittivity profile proposed in

this work reads

$$\varepsilon(z) = 1 + \frac{2(\epsilon - 1)}{1 + \exp\{-[\frac{6}{\pi}n_3(z) - \rho_b^*]\}}, \tag{55}$$

where ϵ is the water bulk dielectric permittivity calculated within MSA approach [46] and $n_3(z)$ represents the smoothed water density profile

$$n_3(z) = \int d\vec{r'}\rho(\vec{r'})\Theta(\vec{r} - \vec{r'})$$

$$= \pi \int_{z-d/2}^{z+d/2} dz'\rho(z')[\frac{d^2}{4} - (z - z')^2]. \tag{56}$$

It is worth mentioning that Eq.(55) is not derived from Eq.(54). By construction Eq.(55) is expected to provide insight into the role that dipole water molecules at realistic water bulk number density and dipolar moment play in the dielectric permittivity properties of electrolyte aqueous solutions near a charged plate. Interestingly, a more accurate description of the structural and dielectric properties of liquid water (brown line in Fig. 3) yields a highly oscillating behavior of the dielectric permittivity profile $\varepsilon(z)$ near the wall due to the strong water layering formation. Additionally, the local dielectric permittivity $\varepsilon(0)$ predicted at the wall surface is smaller than the corresponding one in bulk solution. This is a consequence of the strong influence of water polarization on the dielectric properties of the electrical double layer near the wall. On the other hand, the dielectric permittivity profile $\varepsilon(z)$ decays asymptotically to the experimental water bulk dielectric permittivity value as expected. The weak dependence of the dielectric permittivity profile $\varepsilon(z)$ on the electric field of the wall arises from the behavior of the smoothed water density profile appearing in the rhs of Eq.(55).

The importance of modeling water molecules at realistic density and dipole moment values is further illustrated in Fig.3, where solvent molecules with lower dipole moment values were considered (blue, green, read and black lines). It is seen that the oscillating behavior, the bulk dielectric permittivity and the effects of the solvent polarization at the wall surface of the dielectric permittivity profile $\varepsilon(z)$ strongly depend on the value of the solvent dipole moment. The lower the solvent dipole moment, the smaller the amplitude of oscillation and the prediction of the dielectric permittivity in bulk and at the wall

surface. Clearly, these dielectric inhomogeneities affecting the EDL's properties cannot be captured by unpolar electrolyte models in which the solvent dielectric permittivity is treated as a continuum medium with permanent dielectric permittivity. To our knowledge, there is no experimental data available to compare with our results on the variation of the dielectric permittivity with the distance from the charged wall and the polarity of the solvent.

B.   HS ion-dipole mixture near the planar charged surface

In this subsection, we present the results for a mixture of monovalent ions and solvent dipoles considered in the previous subsection near a charged hard wall. The size of ions was set to be equal to the one of dipoles, i.e. $d = 2.75\,\mathring{A}$ and the dimensionless charge of monovalent ions at room temperature equal $q^* = 14.3$. We study the polarization effects on structural, dielectric and thermodynamic properties of EDLs near a charged wall using PSCDFT and USCDFT. In doing so the bulk water dielectric permittivity constant was set equal to $\varepsilon = 79.7$ in USCDFT to establish the correct correspondence between PSCDFT and USCDFT results.

1.   Structural properties: Density and mean electrostatic potential profiles

The ionic and dipole density profiles were analyzed to provide valuable information on the structural arrangements and layering formation of ion and solvent water molecules near the plate. Figs. 4 and 5 show the scaled density profiles $\{\rho_i(z)/\rho_{i,b}\}$ $(i = 1, 2, 3)$ predicted for electric potentials $\varphi_0^* = 0.25$ ($\varphi_0 = 6.4\,mV$) and $\varphi_0^* = 1.0$ ($\varphi_0 = 25.7\,mV$) on the charged plate, respectively. The notation $+q$ and $-q$ marks the scaled density profiles for positively charged ions $\rho_1(z)/\rho_{1,b}$ and negatively charged ions $\rho_2(z)/\rho_{2,b}$, respectively, whereas m and HS represents the scaled solvent density profile for the dipole component $\rho_3(z)/\rho_{3,b}$ in PSCDFT and the neutral hard-sphere component in USCDFT, respectively. In these Figures, the position of the peaks describes the electrolyte shells, e.g. the separation distance from the wall with highest particle density numbers, whereas the height of the scaled density peaks represents the augmentation or reduction of the local density on the shells with respect to the bulk density value. For instance, scaled peak heights

larger than one represent particle accumulation whereas lower values than one represent particle depletion due to the presence of the charged plate. Fig.4 shows that the reorientation of the dipole water molecules induced at low electrostatic potential ($\varphi_0^* = 0.25$) is negligible, producing an insignificant difference between the density profiles predicted by PSCDFT and USCDFT. On the other hand, a high electrostatic potential ($\varphi_0^* = 1.0$) causes a quantitative discrepancy between PSCDFT and USCDFT results due to stronger water polarization effects. The dominant role of the water crowding contributions to the ionic potential of mean force is shown in Fig.5 where an accumulation in the first and second ionic shells of both positive (red and black lines) and negative (blue and orange lines) ions is affected by the water excluded volume interaction (green and brown lines) that pushes many ions toward the plate surface. Moreover, negative ions exhibit higher accumulation than the positive ions. The attractive electrostatic interaction between the positive plate charge density and the negative ion charge species pushes negative ions toward the plate. In contrary, the repulsive electrostatic interaction acting between the positive plate charge density and the positive ion charge species pushes positive ions in the opposite direction. A different scenario is observed at intermediate-range scaled distances z/d, approximately between 5 and 25, where the short-range water crowding effects become negligible (see green and brown lines) and the electrostatic interaction dominates the behavior of the ionic density profiles in this regime. Consequently, the depletion of negative ions and accumulation of positive ions is observed after the second ionic shell. For scaled distances larger than 25 both ion and dipole species are unaffected by the presence of the charged plate where the local particle density profiles reach the bulk (homogeneous) density limit. For high wall electric potentials, Fig. 5 shows that both water crowding and water polarization affect the electrical double layer properties near the plate. The comparison between Figs.4 and 5 reveals that high electric plate potentials generate higher accumulation of negative ions and depletion of positive ions, as well as slower asymptotic decay to the bulk density values compared with those results obtained at low electric potentials. Interestingly, the green lines in Figs. 4 and 5 show that the wall charge density affects the ion number density profiles, whereas it does not induce significant changes on the dipole number density profiles.

This behavior of the ion and dipole density profiles influences the water polarization and the intensity of plate electric field on the macroscopic mean electrostatic potential

profiles $\varphi^*(z)$. While Fig.6 shows that the water polarization does not affect the asymptotic monotonic decay behavior of the mean electrostatic potentials, it strongly influences these profiles near the wall where they manifest a highly oscillating behavior. This is associated with the last contribution in rhs of Eq.(41) which involves the integration of the highly oscillating electric polarization profile $P^*(z)$. As a result, PSCDFT (red and green lines) predicts repulsive as well as attractive potential interactions near the wall due to the strong oscillatory behavior of the polarization profiles. A different behavior is predicted by USCDFT, where the purely repulsive total electric potential acting on the ions (black and blue lines) displays a relatively smooth behavior. Both DFT approaches predict higher asymptotic decay rate of the repulsive mean electrostatic potentials for larger plate electric potentials. In good agreement with experiments[70], our approach predicts the position of the first ionic shell around the particle size. It also predicts a layers formation of cations and anions even when the plate surface has a relatively weak charge density and the aqueous solution has a low electrolyte concentration.

2. Dielectric properties: Orientational order parameter and water polarization profiles

In this subsection different values of plate electric potentials were used to calculate the orientational order parameter profiles $\eta_{10}(z) = <\cos\theta>$ for dipolar water species with (red lines) and without (blue lines) the presence of $10\,mM$ monovalent salt. This analysis provides insight into the effects of the salt concentration on the interaction between the electric field generated by the plate and water dipoles. Figs.7a) and 7b) display the results corresponding to water dipole moment $m = 2.22\,D$ ($m^* = 2.4$ in dimensionless units) and wall electrical potentials $\varphi_0 = 6.4\,mV$ and $\varphi_0 = 25.7\,mV$, respectively. For low and high values of the electric potentials, the presence of salt does not affect the structure (e.g. the position of the peaks) of the order parameter profiles, but induces higher water dipole alignment (e.g. the height of the peaks) along the electric field direction near the plate. The presence of salt also affects the asymptotic decay behavior of the order parameter profiles. The strong salt screening generated by the electrical double layer on the long-range electrostatic interaction between water dipoles and the electric field of the wall avoids the orientational dipole ordering along the direction of the wall electric field. As a result, the corresponding profiles vanish at large distances from the plate.

In contrary, the bulk orientational order parameter in pure dipole fluids is non-zero as explained in the previous subsection. A different dipolar solvent was also considered for comparison purposes. Figs. 8a) and 8b) display the orientational order parameter profiles corresponding to a lower value of the solvent dipole moment $m = 0.93\,D$ ($m^* = 1.0$ in dimensionless units) and wall electric potentials $\varphi_0^* = 6.4\,mV$ and $\varphi_0 = 25.7\,mV$, respectively. In this case the weaker electrostatic interaction between the electric field of the wall and the solvent dipole moments reduces the number of peaks and the dipole ordering along the direction of the electric field.

The orientational order parameter $\eta_{10}(z)$ and the number density $\rho_3(z)$ profiles described above for ion-dipole electrolyte solutions were used to analyze the salt effects on water polarization profiles $P(z)$ near a plate at different wall electric potentials (see Eq.(35)). The comparison between Figs. 2 and 9 reveals different asymptotic behaviors between the water polarization profiles predicted with and without the presence of salts. Pure polar water fluids generate a permanent, non-zero bulk orientational order parameter, which is proportional to the bulk water polarization, whereas the presence of ions in water vanishes the bulk water polarization for all wall electric potentials. This is due to the asymptotic behavior of the orientational order parameter and water number density profiles explained above. The polarization profiles $P^*(z)$ predicted by PSCDFT and USCDFT were depicted in Fig.10 to further compare the dielectric properties of polar and unpolar fluids. The latter is calculated using $P(z) = \frac{(\varepsilon - 1)}{4\pi}E(z)$. Both PSCDFT and USCDFT results manifest a similar asymptotic decay behavior. However, the polarization profile predicted by USCDFT is a smooth function, even near to the plate, due to the behavior of the Maxwell electric field $E(z)$, coming from the smoothing integration of the total charge profile, i.e. $E(z) = -\frac{4\pi}{\varepsilon}\int_z^\infty Q(z')dz'$. In contrast, the electric polarization $P^*(z)$ predicted by PSCDFT is a highly oscillating function due to the strong orientation of the water dipoles along the electric field near the plate.

3. *Thermodynamic properties: Differential Capacitance, excess adsorption and surface tension*

Eq.(40) defines the electroneutrality of the system, which depends on the ion density profiles $\rho_1(z)$ and $\rho_2(z)$ analyzed in the previous subsection. This equilibrium condition establishes a direct relationship between the wall charge density σ^* and the wall electric

potential φ_0^*. Thus, this relationship was studied using PSCDFT and USCDFT to provide insight into the water polarization effects on the wall charge density as a function of the potential φ_0^* (see Fig.11). It was found that for a given potential φ_0^*, the charge density predicted by PSCDFT is always higher than that predicted by USCDFT. In particular, the water polarization effects increase when increasing the potential φ_0^*. This phenomenon is due to the wall electric potential effects on the water orientational order parameter and polarization as explained above. Moreover, the relationship between the charge density and the potential φ^* dominates the behavior of the differential capacitance $C = d\sigma^*/d\varphi_0^*$, which basically represents the ability of a body to store charge under changes on the potential φ_0^*. Fig.12 shows an enhancement of differential capacitance predicted by USCDFT due to the water polarization. When the potential φ_0 is increased from 0 to $25.7\,mV$, the corresponding capacitance C predicted by PSCDFT and USCDFT increase around $18\,\%$ and $13\,\%$, respectively. The higher capacitance observed in polar fluids is attributed to the low dielectric permittivity at the wall (compared to the bulk value), the larger accumulation of negative ions and depletion of positive ions near the charged plate.

The ion and dipole density profiles studied in the previous subsection also dominate the behavior of other relevant thermodynamic properties of the system. Such is the case of the scaled surface excess adsorptions of each species component Γ_i^* ($i = 1, 2, 3$), which represent the excess of the number of particles of each species per unit of area, relative to that in the bulk per unit of area (see Eq.(52)). The water polarization effects on the relationship between the scaled surface excess adsorptions of each species and the potential φ_0^* were examined using PSCDFT and USCDFT (see Fig.13). As expected, water polarization and potential φ_0^* almost do not affect the adsorption of the solvent species Γ_3^* since the dipole density profiles do not depend on these parameters (see previous result sections). A different scenario is observed for the ionic adsorption. Both approaches predict an increase of the adsorption of the negatively charged ions Γ_1^* and a decrease of the adsorption of the positively charged ions Γ_2^* when increasing the electric potentials φ_0^*. This is due mainly to the effects of the electric field generated by the wall, which increases the accumulation of negative ions and the depletion of positive ions as explained above. Additionally, the water polarization considered in PSCDFT enhances the magnitudes of the scaled adsorptions for both ion species compared to USCDFT results.

Another relevant thermodynamic property of the system analyzed in this work is the wall-fluid surface tension γ. This quantity basically represents an excess grand canonical potential per unit of surface area required to immerse the wall in a liquid when the chemical potentials of mixture species are fixed (Eq.(53)). Fig.14 shows the influence of the charge density σ^*, the ionic concentration and water polarization on the wall-fluid surface tension γ^*. The red and blue lines correspond to PSCDFT predictions, whereas the green line represents USCDFT predictions. For convenience, these results were re-scaled to the wall-fluid surface tension of the neutral HS solvent $\gamma_{HS}^* = 1.0168$ (or $\gamma_{HS} = 5.50 \cdot 10^{-2} \frac{N}{m}$ in dimensional units). A slight influence of the surface charge density is observed on the surface tension for both $c = 0$ and $c = 10\,mM$ ionic concentrations. When the value of the surface charge density σ increases from 0 to $5.9 \cdot 10^{-3}\,\frac{C}{m^2}$ (0.04 in dimensionless units) the corresponding surface tension γ^* only increases around $0.03\,\%$. This phenomenon is attributed to the low ion concentrations and small charge densities on the plate considered in this work. The ionic number density profiles $\rho_1(z)$ and $\rho_2(z)$ and the dipole orientational order parameter profile $\eta_{10}(z)$ are much smaller than the water number density profile $\rho_3(z)$ and, consequently, the surface tension γ depends on the latter one mainly. As a result, the surface tension predicted for polar fluids γ is similar to that of the pure HS solvent γ_{HS}. In particular, the electric field of the wall has a negligible effect on the water number density profile and, therefore, on the surface tension as well. In that case, the absence of electrostatic oscillation predicted by PSCDFT is responsible for a short-range attraction observed in experiments[70]. On the other hand, the addition of the electrolyte to water is well known to cause an increase of the vapor-liquid surface tension [71]. This behavior is displayed in Fig. 14 where the rise of ionic concentration from $c = 0\,mM$ to $c = 10\,mM$ leads to an increase of $0.15\,\%$ in the wall-liquid surface tension, approximately. To further discuss the effects of water polarization, the ratio between the wall-fluid surface tension predicted by PSCDFT and USCDFT in presence of $10\,mM$ salt concentration is presented in Fig.15. While the surface tension γ^* predicted by PSCDFT slightly increases (red line), the one predicted by USCDFT slightly decreases (green line) with increasing the surface charge density σ^* (Fig.14). We have noticed that our computational scheme cannot be used in the present form to see whether there is still a rise in the surface tension at higher ion concentrations due to numerical convergence issues.

IV.   CONCLUSIONS

In this paper a Polar Solvation Classical Density Functional Theory (PSCDFT) was introduced to provide a better understanding on the effects of water concentration and dipolar moment, electrolyte concentration, and plate surface charge density on structural and thermodynamic properties of ionic electrical double layers near a uniformly charged hard wall. A crucial step in arriving to this understanding lied in describing water molecules at experimentally known size, concentration and dipolar moment as well as to account for the detailed description of the ion-ion, ion-dipole and dipole-dipole interactions. This is possible because PSCDFT is based on a DFT approach that uses a refined ion-dipole electrolyte aqueous solution model along a novel combination of accurate and efficient approximate approaches, e.g. the PB equation, the MSA-DCF and the WBII version of FMT. In fact, PSCDFT is a straightforward extension of the numerically and experimentally validated Unpolar Solvation Classical Functional Density Functional Theory (USCDFT) recently introduced by M. Marucho and collaborators to describe symmetric solutes immersed in unpolar electrolyte aqueous solutions.

The proposed PSCDFT was used to calculate the equilibrium profiles of the number densities of ions and dipoles, polarization, dielectric permittivity and mean electric potential. These profiles were employed to compute the differential capacitance, excess adsorptions and wall-fluid surface tension. The obtained results were compared with those corresponding to the pure dipolar model and unpolar primitive solvent model of electrolyte aqueous solutions to understand the role that water crowding and polarization effects play on the structural and thermodynamic properties of these systems.

It is shown that increasing the plate electric potential strengthens the oscillations of the orientational order parameter and the polarization profiles. Additionally, it widens these profiles near a charged wall. It also increases the depletion of positive ions, the accumulation of negative ions and slightly increases the wall-fluid surface tension. It is also found that increasing the electrolyte concentration increases the wall-fluid surface tension. A qualitatively different behavior of the order parameter and polarization profiles has been found between pure dipolar fluids and ion-dipole mixture electrolyte solutions. In the former case, the electric field generated by the charge plate is not screened, making the order parameter and polarization profiles decay oscillatory to the non-zero bulk values.

In contrary, the latter case shows that the electrical double layer screens the electric field of a charged plate. Thus, the order parameter and polarization profiles vanish to zero in the bulk limit.

We compared the results predicted by PSCDFT and USCDFT. It was found that the discrepancy in the density profiles predicted by these two approaches increases with increasing the electrostatic plate potential. We observed that the effects of water polarization enhanced the magnitudes of the scaled adsorptions for both ion species as compared to USCDFT results. Additionally, the results predicted by PSCDFT and USCDFT manifest a similar asymptotic decay behavior of the polarization profiles. However, the polarization profiles predicted by USCDFT have a smooth monotonic decay behavior, even near to the plate. In contrast, the one predicted by PSCDFT possesses marked oscillations due to the strong orientation of the water dipoles along the electric field direction near the plate. Overall, PSCDFT predictions are in agreement with available experimental data.

It is worth mentioning that our method can be extended to study the effects of tunable solvent dipole moment on the properties of nanoporous electrodes in biological cells or vessels. On the other hand, the electrostatic potential used in the present work for describing many biological systems is small compared to that used in other applications including supercapacitors [76]. Broader PSCDFT applications will require the consideration of higher electrolyte concentrations, asymmetric particle sizes, multivalent ions, and more complex geometries of the EDLs. Additionally, coupling the PSCDFT with other master equations will allow to study the dynamic properties of EDLs at solid-liquid interface. In particular, a Navier-Stokes-like theory together with the PSCDFT may provide a theoretical framework to describe an electrokinetic phenomena that arise from the application of the tangential electric field to the EDL. This includes, for example, the ionic conductance, electro-osmic mobility and stream current [75]. Work along these directions is currently carrying on in our Lab.

Acknowledgements

Appendix A: The Density Functional Theory

In this Appendix the Density Functional Theory for a single-component fluid [57, 58] is introduced to describe an inhomogeneous system under the effects of an external field $V^{(ext)}(r)$. The grand canonical potential for this system can be written in terms of an unknown density $\rho(r)$ as follows

$$\Omega[\rho] = F[\rho] - \int [\mu - V^{(ext)}(\vec{r})]\rho(\vec{r})d\vec{r}, \tag{A1}$$

where $F[\rho]$ is an intrinsic Helmholtz free-energy energy functional and μ the chemical potential.

The grand canonical potential can be conveniently decomposed in two contributions [57]

$$\Omega[\rho] = \Omega[\rho_b] + \Delta\Omega[\rho], \tag{A2}$$

where $\Omega[\rho_b]$, ρ_b, and $\Delta\Omega[\rho]$ represent the grand canonical potential in bulk phase, the bulk density, and the excess over the bulk contribution, respectively. In addition, the excess grand canonical potential can be written in terms of an ideal gas part $\Delta\Omega_{id}$, an external potential part $\Delta\Omega_{ext}$, and an intrinsic part $\Delta\Omega_{int}$ (which accounts for the intermolecular interactions within the fluid) as follows

$$\Delta\Omega[\rho] = \Delta\Omega_{igas}[\rho] + \Delta\Omega_{ext}[\rho] + \Delta\Omega_{int}[\rho]. \tag{A3}$$

with

$$\Delta\Omega_{igas}[\rho] = k_B T \int d\vec{r}[\rho(\vec{r})\ln(\frac{\rho(\vec{r})}{\rho_b}) - \rho(\vec{r}) + \rho_b], \tag{A4}$$

$$\Delta\Omega_{ext}[\rho] = \int d\vec{r}V_{ext}(\vec{r})\rho(\vec{r}), \tag{A5}$$

$$\Delta\Omega_{int}[\rho] = k_B T \int \int d\vec{r}d\vec{r'}C(\vec{r},\vec{r'})\Delta\rho(\vec{r})\Delta\rho(\vec{r'}), \tag{A6}$$

where k_B is the Boltzmann constant, T the temperature, $\Delta\rho(\vec{r}) = \rho(\vec{r}) - \rho_b$ and $C(\vec{r},\vec{r'})$ a functional of the density

$$C(\rho;\vec{r},\vec{r'}) = \int_0^1 d\alpha(\alpha - 1)c^{(2)}([\rho_\alpha(\vec{r})];\vec{r},\vec{r'}). \tag{A7}$$

In the latter equation, $c^{(2)}([\rho_\alpha]; \vec{r}, \vec{r'})$ represents the two-particle direct correlation function evaluated at the density $\rho_\alpha(\vec{r}) = \rho_b + \alpha\Delta\rho(\vec{r})$.

While the functional in Eqs.(A2)-(A7) is formally exact, an approximation for the unknown direct correlation function $c^{(2)}([\rho_\alpha(\vec{r})]; \vec{r}, \vec{r'})$ is needed. It is usually approximated by the direct correlation function corresponding to the homogeneous fluid

$$c^{(2)}([\rho_\alpha(\vec{r})]; \vec{r}, \vec{r'}) = c^{(2)}([\rho_b]; \vec{r}, \vec{r'}), \tag{A8}$$

where ρ_b is the bulk density of the homogenous fluid. According to Eqs.(A6)-(A8), the following expression to calculate the intrinsic term can be obtained

$$\Delta\Omega_{int}[\rho] = -\frac{k_B T}{2} \int\int d\vec{r} d\vec{r'} c^{(2)}([\rho_b]; \vec{r}, \vec{r'})\Delta\rho(\vec{r})\Delta\rho(\vec{r'}). \tag{A9}$$

The unknown density of the system is calculated from the equilibrium condition

$$\frac{\delta\Omega[\rho]}{\delta\rho(\vec{r})} = 0, \tag{A10}$$

which provides the following integral equation solution

$$\rho(\vec{r}) = \rho_b \exp\{-\beta V_{ext}(\vec{r}) + \int d\vec{r} c^{(2)}([\rho_b]; \vec{r}, \vec{r'})\Delta\rho(\vec{r})\}. \tag{A11}$$

Appendix B: Expressions for the functions c_{ii}, c_{id} and c_{dd}

In this Appendix the explicit expressions of the functions c_{ij}, c_{id}, and c_{dd} appearing in Eqs.(14),(15),(16) are provided. These functions vanish outside the hard-core (i.e. for $r \equiv r_{12} > d$), whereas inside the hard-core they are given by the expressions

$$c_{ij}(\vec{r}_1, \vec{r}_2) = \xi_i \xi_j c_{ii}^{(000)}(r), \tag{B1}$$

$$c_{id}(\vec{r}_1, \vec{r}_2, \omega_2) = \xi_i c_{id}^{(011)}(r)\Phi^{(011)}(\hat{r}_{12}, \hat{m}_2), \tag{B2}$$

$$c_{dd}(\vec{r}_1, \omega_1, \vec{r}_2, \omega_2) = c_{dd}^{(110)}(r)\Phi^{(110)}(\hat{m}_1, \hat{m}_2) + c_{dd}^{(112)}(r) \cdot \Phi^{(112)}(\hat{r}_{12}.\hat{m}_1, \hat{m}_2) \tag{B3}$$

The rotational invariant $\Phi^{(110)}$ appearing in Eq.(B3) is defined as [56]

$$\Phi^{(110)}(\hat{m}_1, \hat{m}_2) = (\hat{m}_1 \cdot \hat{m}_2), \tag{B4}$$

whereas the rotational invariants $\Phi^{(011)}$ and $\Phi^{(112)}$ were defined in Eq.(4).

The radial functions $c_{ii}^{(000)}(r)$, $c_{id}^{(011)}(r)$, $c_{dd}^{(110)}(r)$, $c_{dd}^{(112)}(r)$ introduced in Eqs. (B1), (B2), (B3) are calculated using the following formulas [72]

$$c_{ii}^{(000)}(r) = C_{ii}(r), \tag{B5}$$

$$c_{id}^{(011)}(r) = C_{id}(r) - \frac{1}{r^2} \int_0^r dr' r' C_{id}(r'), \tag{B6}$$

$$c_{dd}^{(110)}(r) = C_{dd}(r) - 2D_{dd}(r), \tag{B7}$$

$$c_{dd}^{(112)}(r) = C_{dd}(r) + D_{dd}(r) - \frac{3}{r^3} \int_0^r dr' r'^2 [C_{dd}(r') + D_{dd}(r')], \tag{B8}$$

where $C_{ii}(r)$, $C_{id}(r)$, $C_{dd}(r)$ are radial functions representing polynomial series expansions in powers of r [53]

$$C_{ii}(r) = C_{ii}^{(0)} + C_{ii}^{(1)} r, \tag{B9}$$

$$C_{id}(r) = C_{id}^{(1)} r + C_{id}^{(2)} r^2, \tag{B10}$$

$$C_{dd}(r) = C_{dd}^{(0)} + C_{dd}^{(1)} r + C_{dd}^{(3)} r^3. \tag{B11}$$

The polynomial coefficients introduced in Eqs.(B9),(B10),(B11) are defined as follows

$$C_{ii}^{(0)} = \frac{1}{w_{ii}}[a_1 Q'_{11} + a_2 Q'_{id}], \qquad C_{ii}^{(1)} = \frac{1}{2w_{ii}}[(Q'_{ii})^2 + (Q'_{id})^2], \tag{B12}$$

$$C_{id}^{(1)} = \frac{1}{2w_{id}}[Q'_{ii} Q'_{di} + Q'_{di} Q'_{dd}], \qquad C_{id}^{(2)} = -\frac{1}{6w_{id}}[Q'_{ii} Q''_{di} + Q'_{id} Q''_{dd}], \tag{B13}$$

$$C_{dd}^{(0)} = -\frac{1}{w_{dd}}\{Q''_{dd} - \frac{1}{6}[(Q''_{dd})^2 + (Q''_{di})^2] + \frac{1}{2}[Q''_{dd} Q'_{dd} + Q''_{di} Q'_{di}], \tag{B14}$$

$$C_{dd}^{(1)} = \frac{1}{2w_{dd}}[(Q'_{dd})^2 + (Q'_{di})^2], \qquad C_{dd}^{(3)} = -\frac{1}{24w_{dd}}[(Q'_{dd})^2 + (Q''_{di})^2], \tag{B15}$$

where

$$w_{ii} = 2\pi \rho_{0,b} d^3, \qquad w_{id} = 2\pi(\rho_{i,b} \rho_{3,b})^{\frac{1}{2}} d^3, \qquad w_{dd} = 2\pi \rho_{3,b} d^3, \tag{B16}$$

and $\rho_{0,b} = \rho_{1,b} + \rho_{2,b}$ represents the total ionic bulk density.

The functions $\{Q'_{ij}\}$, $\{Q''_{ij}\}$, a_1, a_2 appearing in Eqs.(B12),(B13),(B14),(B15) are equal to

$$Q'_{ii} = -\frac{1}{2}[(2 - \frac{\beta_6}{D_F})^2 + (\frac{\beta_1}{2D_F})^2], \qquad Q'_{id} = \frac{b_1}{4(D_F)^2}(\beta_6 + \frac{\Lambda_F}{2}), \tag{B17}$$

$$Q'_{di} = -Q'_{id}, \qquad Q'_{dd} = 6 - \frac{12(1 + b_0)}{D_F} + \frac{9}{2}\frac{(1 + b_0)^2}{(D_F)^2} + \frac{(b_1)^2}{8(D_F)^2}, \tag{B18}$$

$$Q''_{ii} = 0, \qquad Q''_{id} = 0, \tag{B19}$$

$$Q''_{di} = 2Q'_{di} + \frac{b_1}{D_F}, \qquad Q''_{dd} = 24 - \frac{30(1 + b_0)}{D_F} + \frac{9(1 + b_0)^2}{(D_F)^2} + \frac{(b_1)^2}{4(D_F)^2}, \tag{B20}$$

$$a_1 = -\frac{1}{2(D_F)^2}(2\beta_6 D_F - \Delta), \quad a_2 = -\frac{b_1}{2(D_F)^2\beta_6}(\beta_3 D_F + \frac{\Delta}{2}), \tag{B21}$$

where β_3, β_6 β_{12} β_{24}, Δ, Λ_F, D_F and y_1 are functions that only depend on the parameters b_0, b_1, b_2

$$\beta_3 = 1 + \frac{b_2}{3}, \qquad \beta_6 = 1 - \frac{b_2}{6}, \qquad \beta_{12} = 1 + \frac{b_2}{12}, \qquad \beta_{24} = 1 - \frac{b_2}{24}, \tag{B22}$$

$$\Delta = (\beta_6)^2 + \frac{(b_1)^2}{4}, \qquad \Lambda_F = (1 + b_0)b_2 + \frac{(b_1)^2}{2}, \tag{B23}$$

$$D = \frac{1}{2}[(1 + b_0)\beta_6 - \frac{(b_1)^2}{12}], \qquad y_1 = \frac{\beta_6}{(\beta_{12})^2}. \tag{B24}$$

The numerical values of the parameters b_0, b_1 and b_2 are obtained from the solution of the set of nonlinear equations [53]

$$\begin{cases} (a_1)^2 + (a_2)^2 = (d_0)^2, \\\\ -a_1 K_{di} + a_2(1 - K_{dd}) = -d_0 d_2, \\\\ (K_{di})^2 + (1 - K_{dd})^2 - (y_1)^2 = (d_2)^2 \end{cases} \tag{B25}$$

where

$$K_{\alpha\beta} = -\frac{1}{2}Q'_{\alpha\beta} + \frac{1}{6}Q''_{\alpha\beta}, \tag{B26}$$

and the parameters d_0 and d_2 are obtained from the initial input data of the theory

$$(d_0)^2 = 4\pi\beta e^2\rho_{0,b}d^2, \qquad (d_2)^2 = \frac{4\pi}{3}\beta m^2\rho_{3,b}. \tag{B27}$$

Once the parameters b_0, b_1, b_2 are found, all the functions $\{Q'_{ij}\}$, $\{Q''_{ij}\}$, a_1, a_2 appearing in Eqs.(B12),(B13),(B14),(B15) can be calculated.

The function $D_{dd}(r)$ introduced in Eqs.(B7),(B8) is equal to [72]

$$D_{dd}(r) = D_{dd}^{(0)} + D_{dd}^{(1)}r + D_{dd}^{(3)}r^3, \tag{B28}$$

where

$$D_{dd}^{(0)} = \frac{b_2}{w_{dd}}A_0(-\frac{b_2}{12}), \quad D_{dd}^{(1)} = \frac{b_2}{w_{dd}}A_1(-\frac{b_2}{12}), \quad D_{dd}^{(3)} = \frac{b_2}{w_{dd}}A_3(-\frac{b_2}{12}), \tag{B29}$$

whereas

$$A_0(\eta) = -\frac{(1+2\eta)^2}{(1-\eta)^4}, \qquad A_2(\eta) = \frac{6\eta(1+\frac{1}{2}\eta)^2}{(1-\eta)^4}, \qquad A_3(\eta) = -\frac{\eta(1+2\eta)^2}{2(1-\eta)^4} \tag{B30}$$

are the coefficients in the polynomial solution of Percus-Yevick direct correlation function inside the hard-core [73]

$$c_2^{(PY)}(r,\eta) = A_0 + A_1r + A_3r^3,$$

where $\eta = \frac{\pi}{6}\rho d^3$ (i.e. $D_{dd}(r) = (b_2/w_{dd})c_2^{(PY)}(r,-b_2/12)$).

Finally, the substitution of the expressions (B9),(B10),(B11),(B28) into (B5),(B6),(B7),(B8) yields

$$c_{ii}^{(000)}(r) = B_1 + B_2r, \tag{B31}$$

$$c_{id}^{(011)}(r) = B_3r + B_4r^2, \tag{B32}$$

$$c_{dd}^{(110)}(r) = B_5 + B_6r + B_7r^3, \tag{B33}$$

$$c_{dd}^{(112)}(r) = B_8r + B_9r^3, \tag{B34}$$

where

$$B_1 = C_{ii}^{(0)}, \quad B_2 = C_{ii}^{(1)}, \quad B_3 = \frac{2}{3}C_{id}^{(1)}, \quad B_4 = \frac{3}{4}C_{id}^{(2)}, \tag{B35}$$

$$B_5 = C_{dd}^{(0)} - 2D_{dd}^{(0)}, \quad B_6 = C_{dd}^{(1)} - 2D_{dd}^{(1)}, \quad B_7 = C_{dd}^{(3)} - 2D_{dd}^{(3)}, \tag{B36}$$

$$B_8 = \frac{1}{4}(C_{dd}^{(1)} + D_{dd}^{(1)}), \quad B_9 = \frac{1}{2}(C_{dd}^{(3)} + D_{dd}^{(3)}). \tag{B37}$$

Appendix C: Expression for the functions $\varphi_{res}^{(qq)}$, $\varphi_{res}^{(qd)}$, $E_{res}^{(qd)}$, and $E_{res}^{(dd)}$.

The following expansions of the rotational invariants $\Phi^{(011)}$, $\Phi^{(110)}$ and $\Phi^{(112)}$

$$\Phi^{(011)}(\hat{r}_{12}, \hat{m}_2) = \frac{4\pi}{3} \sum_{n=-1}^{1} (-1)^n Y_{1,n}(\omega_{12}) Y_{1,-n}(\omega_2), \tag{C1}$$

$$\Phi^{(110)}(\hat{m}_1, \hat{m}_2) = \frac{4\pi}{3} \sum_{n=-1}^{1} (-1)^n Y_{1,n}(\omega_1) Y_{1,-n}(\omega_2), \tag{C2}$$

$$\Phi^{(112)}(\hat{r}_{12}, \hat{m}_1, \hat{m}_2) = 4\pi(\frac{8\pi}{15})^{\frac{1}{2}} \sum_{n_1,n_2,n_3} c(123; n_1, n_2, n_3) Y_{1,n_1}(\omega_1) Y_{1,n_2}(\omega_2) Y^*_{2,n_3}(\omega_{12}) \tag{C3}$$

were used to write the angular integrations appearing in Eq.(43) in the terms of spherical harmonics [56], where $|n_1| \leq 1$, $|n_2| \leq 2$, $n_3 = n_1 + n_2$, $C(123; n_1, n_2, n_3)$ are the Clebsch-Gordan coefficients in the Rose convention [74], and ω_{12} denotes the orientation of the intermolecular axis in the space-fixed coordinate system.

Substituting Eqs. (1),(2),(3), (C1), (C2),(C3), (B1), (B2), (B3) into Eq.(43) and using the spherical harmonics orthogonality properties, we obtain

$$\Delta\Omega_{res}[Q, P] = -\frac{1}{2\beta} \int d\vec{r}_1 d\vec{r}_2 Q(\vec{r}_1) Q(\vec{r}_2) \chi^{(ii)}(\vec{r}_1, \vec{r}_2)$$

$$-\frac{1}{\beta} \int d\vec{r}_1 d\vec{r}_2 Q(\vec{r}_1) P(\vec{r}_2) \chi^{(id)}(\vec{r}_1, \vec{r}_2) - \frac{1}{2\beta} \int d\vec{r}_1 d\vec{r}_2 P(\vec{r}_1) P(\vec{r}_2) \chi^{(dd)}(\vec{r}_1, \vec{r}_2), \tag{C4}$$

where the following expressions for the functions $\chi^{(qq)}$, $\chi^{(qd)}$, $\chi^{(dd)}$ were calculated

$$\chi^{(qq)}(\vec{r}_1, \vec{r}_2) = \frac{1}{e^2}[B_1 + B_2 r_{12} + \frac{\beta e^2}{r_{12}}] \Theta(d - r_{12}),$$

$$\chi^{(qd)}(\vec{r}_1, \vec{r}_2) = \frac{1}{em}[B_3 r_{12} + B_4 r_{12}^2 + \frac{\beta em}{r_{12}^2}] P_1(\cos\theta_{12}) \Theta(d - r_{12}),$$

$$\chi^{(dd)}(\vec{r}_1, \vec{r}_2) = \frac{1}{m^2}[B_5 + B_6 r_{12} + B_7 r_{12}^3 -$$

$$(2B_8 r_{12} + 2B_9 r_{12}^3 + 2\frac{\beta m^2}{r_{12}^3}) P_2(\cos\theta_{12})] \Theta(d - r_{12}). \tag{C5}$$

It is seen that Eq.(C4) can be transformed to Eq.(44), where

$$\varphi_{res}^{(qq)}(z_1) = -\frac{1}{\beta} \int d\vec{r}_2 Q(\vec{r}_2) \chi^{(qq)}(\vec{r}_1, \vec{r}_2), \qquad \varphi_{res}^{(qd)}(z_1) = -\frac{1}{\beta} \int d\vec{r}_2 P(\vec{r}_2) \chi^{(qd)}(\vec{r}_1, \vec{r}_2), \tag{C6}$$

$$E_{res}^{(dq)}(z_1) = \frac{1}{\beta} \int d\vec{r}_2 Q(\vec{r}_2) \chi^{(qd)}(\vec{r}_1, \vec{r}_2), \qquad E_{res}^{(dd)}(z_1) = \frac{1}{\beta} \int d\vec{r}_2 P(\vec{r}_2) \chi^{(dd)}(\vec{r}_1, \vec{r}_2). \quad \text{(C7)}$$

To write the functions $\varphi_{res}^{(qq)}$, $\varphi_{res}^{(qd)}$, $E_{res}^{(dq)}$, and $E_{res}^{(dd)}$ in terms of one-dimensional integrals, the integration volume in Eqs.(C6)-(C7) was written in the thermodynamical limit

$$\lim_{V_2 \to \infty} \int_{V_2} d\vec{r}_2 ... = \lim_{L \to \infty} \int_{z_0}^{L} dz_2 \int_{0}^{2\pi} d\varphi_2 \int_{0}^{L} dR_2 R_2 ..., \qquad \text{(C8)}$$

where R_2 is the cylinder radius. Upon substitution of Eqs.(C5),(C8) into Eqs. (C6)-(C7), the inequality $|\vec{r}_1 - \vec{r}_2| < d$ imposed by the Heaviside step-function $\Theta(d - r_{12})$ in Eq.(C5) yields the following integration boundary conditions $|z_1 - z_2| < d$ and $0 \leq R_2 \leq \sqrt{d^2 - (z_1 - z_2)^2}$. Using this, the expressions in Eqs.(C6)-(C7) can be transformed as follows

$$\varphi_{res}^{(qq)}(z_1) = -\frac{1}{\beta e^2} \int_{z-d}^{z+d} dz_2 \left\{ \pi[d^2 - (z_1 - z_2)^2]B_1 + \right. \qquad \text{(C9)}$$
$$\frac{2\pi}{3}[d^3 - |z_1 - z_2|^3]B_2 + 2\pi[1 - |z_1 - z_2|]\beta e^2\}Q(z_2) ,$$

$$\varphi_{res}^{(qd)}(z_1) = -\frac{1}{\beta em} \int_{z-d}^{z+d} dz_2 \left\{ \pi[d^2(z_1 - z_2) - (z_1 - z_2)^3]B_3 + \right.$$
$$\frac{2\pi}{3}[d^3(z_1 - z_2) - (z_1 - z_2)|z_1 - z_2|^3]B_4 + 2\pi\beta em[\frac{(z_1 - z_2)}{|z_1 - z_2|} - \frac{(z_1 - z_2)}{d}]\}P(z_2) , \quad \text{(C10)}$$

$$E_{res}^{(qd)}(z_1) = \frac{1}{\beta em} \int_{z-d}^{z+d} dz_2 \left\{ \pi[d^2(z_1 - z_2) - (z_1 - z_2)^3]B_3 + \right.$$
$$\frac{2\pi}{3}[d^3(z_1 - z_2) - (z_1 - z_2)|z_1 - z_2|^3]B_4 + 2\pi\beta em[\frac{(z_1 - z_2)}{|z_1 - z_2|} - \frac{(z_1 - z_2)}{d}]\}Q(z_2) , \quad \text{(C11)}$$

$$E_{res}^{(dd)}(z_1) = \frac{1}{\beta m^2} \int_{z_1-d}^{z_1+d} dz_2 \{ \pi[B_5(d^2 - |z_1 - z_2|^2) + B_6 \frac{2}{3}(d^3 - |z_1 - z_2|^3) +$$
$$B_7 \frac{2}{5}(d^5 - |z_1 - z_2|^5)] + 2\pi[B_8\{3|z_1 - z_2|^2(d - |z_1 - z_2|) - \frac{1}{3}(d^3 - |z_1 - z_2|^3\} +$$
$$B_9\{|z_1 - z_2|^2(d^3 - |z_1 - z_2|^3) - \frac{1}{5}(d^5 - |z_1 - z_2|^5)\}] - 2\pi\frac{\beta m^2}{d^3}(|z_1 - z_2|^2 - d^2)\}P(z_2) \text{(C12)}$$

[1] M.R.Wright, *An Introduction to Aqueous Electrolyte Solutions* (John Wiley & Sons Inc., NY, 2007).

[2] M.A.Shenashe, E.A.Elshehy, S.A.El-Safty, and M.Khairy, Separation and Purification Technology **116**, 73 (2013).

[3] K. E. Barrett, S. M. Barman, S. Boitano, and H. L. Brooks W.F., *Ganong's Review of Medical Physiology* (McGraw-Hill, 2010).

[4] P.Ren, J.Chun, D.G.Thomas, M.J.Schnieders,M.Marucho,J.Zhang, and N.A.Baker, Quart.Rev.Biophys., **45**, 427 (2012).

[5] J.S.Høye, and E.Lomba, J.Chem.Phys. **88**, 5790 (1988).

[6] J.S.Høye, E.Lomba, G.Stell, J.Chem.Phys. **89**, 7462 (1988).

[7] D.Y.C.Chan, D.J.Mitchell, and B.W.Ninham, J.Chem.Phys. **70**, 2946(1979).

[8] S.L.Carnie and D.Y.C.Chan, J.Chem.Soc.FaradayTrans. **78**, 695(1982).

[9] S.L.Carnie and D.Y.C.Chan, J.Chem.Phys. **73**, 2949(1980).

[10] E.Diaz-Herrera, F.Forstmann, J.Chem.Phys. **102**, 9005(2004).

[11] D.Andelman, in *Handbook of Biological Physics. Vol.1, Edited by R.Lipowski and E.Sackmann* (Elsevier,1995).

[12] E.Waisman and J.L.Lebowitz, J.Chem.Phys. **56**, 2999(1972).

[13] E.Waisman and J.L.Lebowitz, J.Chem.Phys. **56**, 3093(1972).

[14] L.Blum, Mol.Phys. **30**, 1529(1975).

[15] K.Hiroike, Mol.Phys. **33**, 1195(1977).

[16] P. Tarazona , Phys. Rev. A **31**, 2672(1985).

[17] Y.Rosenfeld, Phys. Rev. Lett., **63**, 980(1989).

[18] Y.Yu and J.Wu, J.Chem.Phys., **117**, 10156(2002).

[19] R.Roth, R.Evans, A.Lang, and G.Kahl, J. Phys.: Condens. Matter, **14**, 12063(2002).

[20] H.Hansen-Goos, R.Roth, J.Chem.Phys., **124**,154506(2006).

[21] C.N.Patra and S.K.Ghosh, Phys.Rev.E **47**, 4088(1993).

[22] C.N.Patra, J.Chem.Phys. **111**, 9832(1999).

[23] Z.Tang, L.Mier-y-Teran, H.T.Davis, L.E.Scriven and H.S.White, Mol.Phys. **71**, 369 (1990).

[24] B.Medasani,Z.Ovanesyan,D.G.Thomas,M.L.Sushko, and M.Marucho, J.Chem.Phys. **140**,

204510(2014).

[25] Z. Ovanesyan, B. Medasani, M. O. Fenley, G. I. Guerrero-Garcia, M. Olvera de la Cruz, and M. Marucho, J.Chem.Phys. **141**, 225103(2014).

[26] J.Wu, T.Jiang, D,Jiang, Z.Jin, and D. Henderson, Soft Matter **7**, 11222(2011).

[27] Y.Rosenfeld, M.Schmidt, H.Lowen, and P.Tarazona, Phys.Rev.E, **55**,4245(1997).

[28] R.Roth, J.Phys.:Condens.Matter, **22**, 063102(2010).

[29] V.B.Warshavsky and X.Song, Phys.Rev.E, 69, 061113(2004).

[30] V.B.Warshavsky and X.Song, Phys.Rev.E, 73, 031110(2006).

[31] V.B.Warshavsky and X.Song, J.Chem.Phys., 129, 034506 (2008)

[32] V.B.Warshavsky and X.Song, Phys.Rev.B, 79, 014101(2009)

[33] H.Hansen-Goos, R.Roth, J.Phys.:Condens.Matter, **18**,8413(2006).

[34] P.I.Teixeira and M.M.Telo da Gama, J.Phys.: Condens. Matters **3**, 111 (1991).

[35] B.Yang, D.E.Sullivan, B.Tjipto-Margo, and C.G.Grey, Mol.Phys. **76**, 709 (1992).

[36] P.Frodl and S.Dietrich, Phys. Rev. A **45**, 7330 (1992).

[37] P.Frodl and S.Dietrich, Phys.Rev.E **48**, 3741 (1993).

[38] V.B.Warshavsky, T.V.Bykov and X.C.Zeng, J.Chem.Phys. **114**, 504 (2001).

[39] V.B.Warshavsky, and X.C.Zeng, J.Chem.Phys. **117**, 3982 (2002).

[40] V.B.Warshavsky and X.C.Zeng, Phys.Rev.Lett. **89**, 246104(2002).

[41] V.B.Warshavsky and X.C.Zeng, Phys.Rev.E **68**, 011203(2003).

[42] V.B.Warshavsky and X.C.Zeng, Phys.Rev.E **68**, 051203(2003).

[43] V.B.Warshavsky and X.C.Zeng, J.Chem.Phys. **139**, 134502(2013).

[44] I.Szalai and S.Dietrich, Eur.Phys.J. E **28**, 347 (2009).

[45] V.Talanquer and D.W.Oxtoby, J. Chem. Phys. **99**, 4670 (1993).

[46] M.S.Wertheim, J.Chem.Phys. **55**, 4291 (1971).

[47] M.Moradi and G.Rickayzen, Mol.Phys. **68**, 903(1989).

[48] C.N.Patra and S.K.Ghosh, J.Chem.Phys. **106**, 2752(1997).

[49] J.Lischer,T.Arias, J.Phys.Chem.B, **114**, 1946 (2010).

[50] S.Zhao,R.Ramirez,R.Vuilleumier, and D.Borgis, J.Chem.Phys., **134**, 194102 (2011).

[51] A.Oleksy, J.-P.Hansen, J.Chem.Phys. **132**, 204702(2010).

[52] I.Ibagon, M.Bier, and S.Dietrich, J.Chem.Phys. **138**, 214703(2013).

[53] F.Vericat and L.Blum, J.Stat.Phys. **22**, 593(1980).

[54] L.Blum, J.Chem.Phys. **61**, 2129(1974).

[55] L.Blum, Chem.Phys.Lett. **26**, 200(1974).

[56] C.G. Gray and K.E. Gubbins, *The Theory of Molecular Fluids* (Claredon, Oxford, 1984).

[57] R.Evans, in *Fundamentals of Inhomogeneous Fluid, Edited by D.Henderson* (Wiley,1992).

[58] W.F.Saam, and C.Ebner, Phys.Rev.A **15**, 2566(1977).

[59] R.Ramirez,R.Gebauer, M.Mareschal and D.Borgis, Phys.Rev.E, **66**, 031206 (2002).

[60] B.Groh and S.Dietrich, Phys.Rev.E **53**, 2509(1996).

[61] J.F.Lutsko, Adv. Chem.Physics, **144**, 1(2010).

[62] J.D.Jackson, *Classical Electrodynamics* (John Wiley & Sons Inc., NY, 1962).

[63] B.Guillot, J. Mol. Liq., **101**, 219 (2002).

[64] D. P. Fernández, Y. Mulev, A. R. H. Goodwin and J. M. H. Levelt Sengers, J. Phys. Chem. Ref. Data **24**, 33 (1995).

[65] L.D.Landau and E.M.Lifshitz, *Electrodynamics of Continuous Media. Course of Theoretical Physics. Vol.8* (Pergamon Press, Oxford, 1960).

[66] D.J.Bonthuis, S.Gekle, and R.R.Netz, Phys.Rev.Lett, **107**, 166102 (2011).

[67] V.Ballenegger and J.-P.Hansen, J.Chem.Phys., **122**, 114711 (2005)

[68] R.Ramirez and D.Borgis, J.Phys.Chem.B, **109**, 6754 (2005).

[69] A.Oleksy, J.-P.Hansen, Mol.Phys., **107**, 2609(2009).

[70] R. G. Horn, D. F. Evans and B. W. Ninham, J. Phys. Chem., 1988, 92, 3531.

[71] L.Onsager and N.N.T.Samaras, J.Chem.Phys., **2**,528 (1934).

[72] M.F.Golovko and I.A.Protsykevich,Chem.Phys.Lett.**142**, 463(1987).

[73] M.S.Wertheim, Phys.Rev.Lett., **10**, 321 (1963).

[74] M.E. Rose, *Elementary Theory of Angular Momentum* (Wiley, New York, 1957).

[75] X.Kong, J.Jiang, D.Lu, Z.Liu, and J.Wu, J. Phys. Chem. Lett., **5**, 3015 (2014).

[76] D.E.Jiang and J.Z. Wu, Nanoscale, **6** 5545(2014).
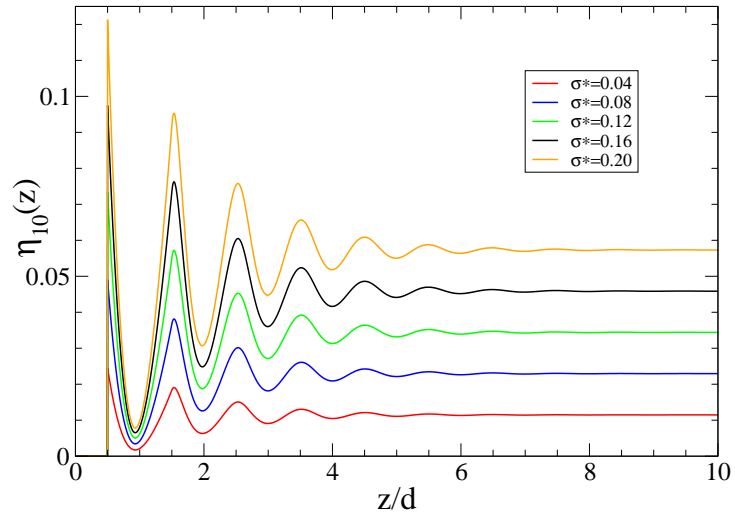
Figure 1: The profiles of the orientational order parameter $\eta_{10}(z) = <\cos\theta>$ of a pure dipolar fluid near a charged plate for different values of the wall charge density σ^*. The number density in a bulk $\rho_b = 0.033/\text{Å}^3$, the dipole moment strength $m = 2.22\, D$.
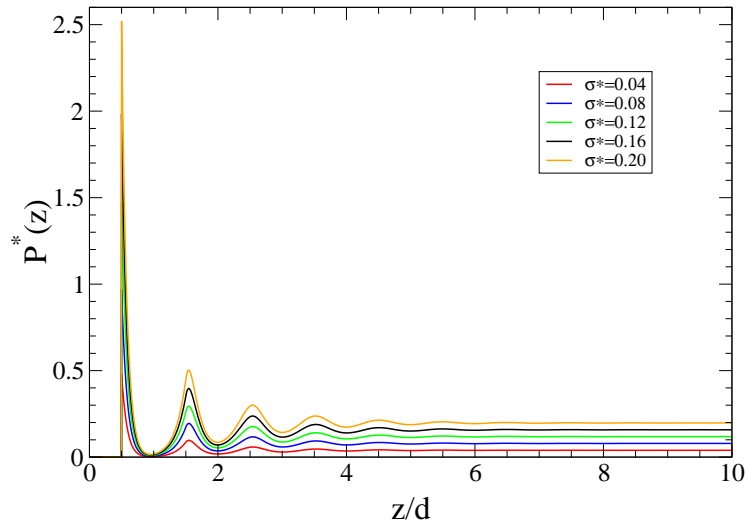
Figure 2: The same as in Fig.1, but for the profiles of the electric polarization $P(z)$.
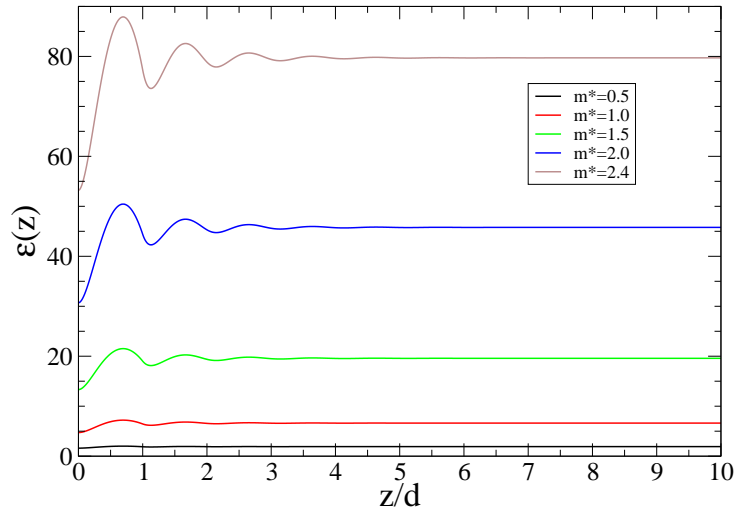
Figure 3: The profiles of the dielectric permittivity $\varepsilon(z)$ of a pure dipolar fluid near a charged hard wall for different values of the dipole moment strength m^* as calculated from Eq.(55). The number density in a bulk $\rho_b = 0.033/\mathring{A}^3$.

a)

b)
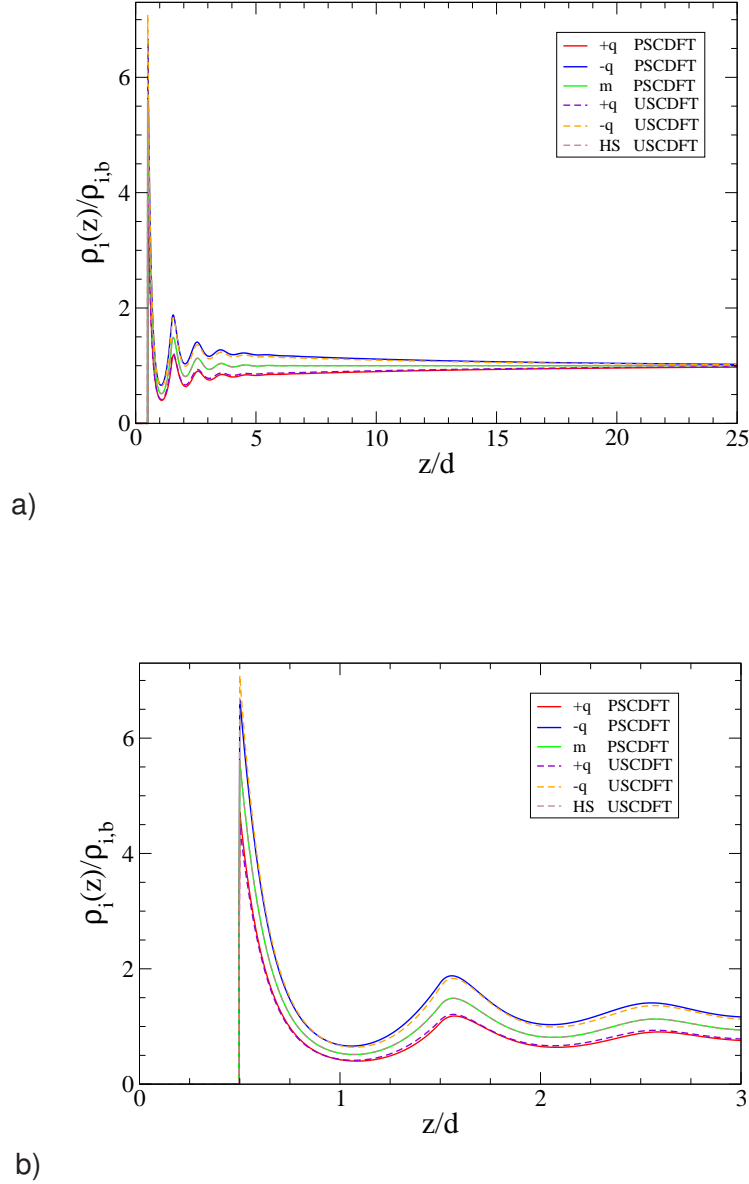
Figure 4: a) The scaled number density profiles of three species of electrolyte solution near a charged hard wall. The results for PSCDFT are compared with the ones for USCDFT. The notations $+q$ and $-q$ mark the density profiles of positively charged ions $\rho_1(z)/\rho_{1,b}$ and negatively charged ions $\rho_2(z)/\rho_{2,b}$, correspondingly , whereas m and HS mark the ones of solvent species $\rho_3(z)/\rho_{3,b}$ for the dipole component in PSCDFT and for a neutral HS component in USCDFT, correspondingly. The ionic concentration $c = 10\,mM$, the wall electric potential $\varphi_0^* = 6.4\,mV$. The dipole moment strength $m = 2.22\,D$ in PSCDFT and the dielectric permittivity $\varepsilon = 79.7$ in USCDFT; b) The same as in Fig.4a. The oscillatory parts of density profiles are displayed with higher resolution.
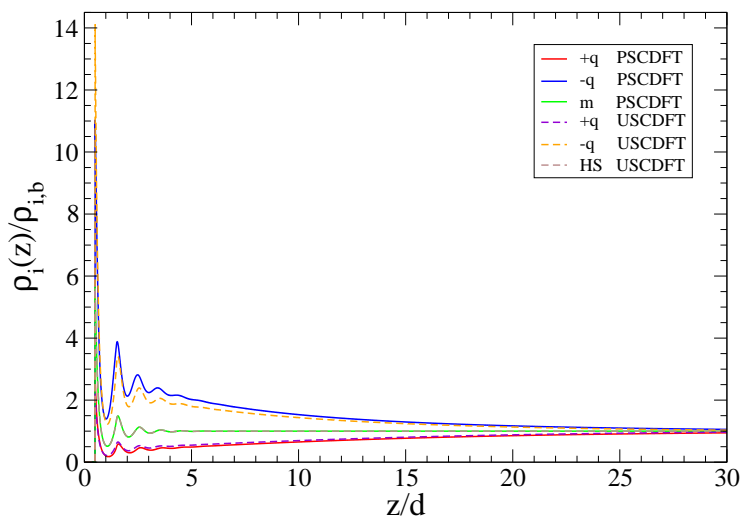
a)
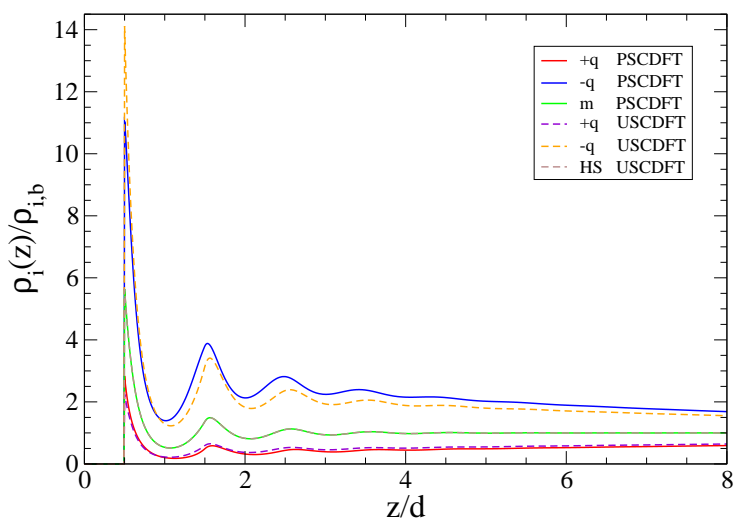
b)

Figure 5: The same as in Fig.4, but for the wall electric potential $\varphi_0 = 25.7\,mV$.
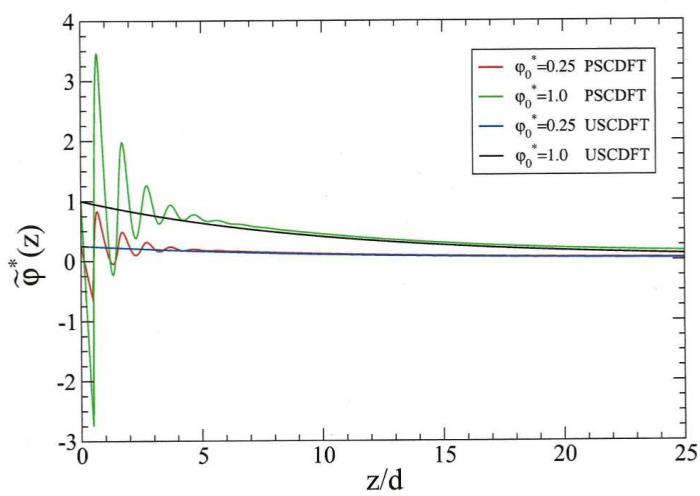
Figure 6: The profiles of the mean electrostatic potential $\tilde{\varphi}^*(z)$ near a charged hard wall for two values of the wall electric potential $\varphi_0 = 6.4\,mV$ and $25.7\,mV$. The results for PSCDFT are compared with the ones for USCDFT. The values of the parameters of an electrolyte solution are the same as the ones in Fig.4.
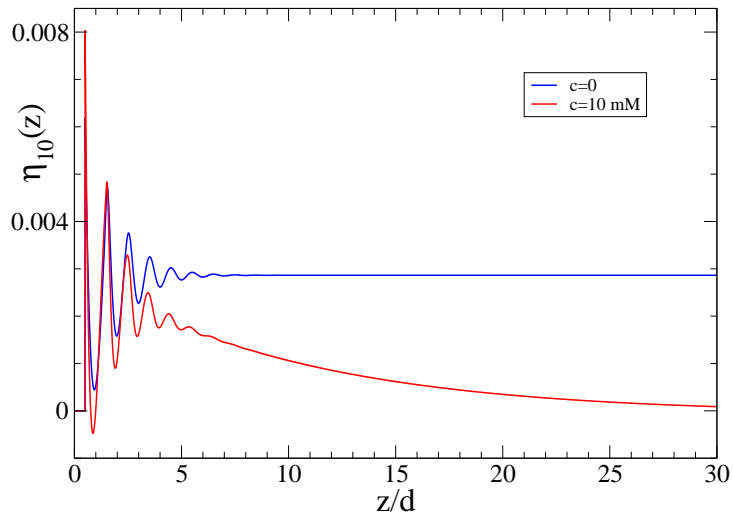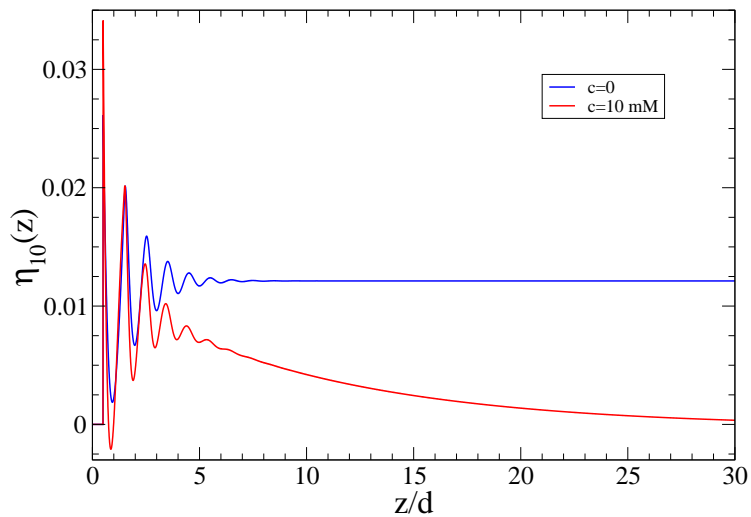
Figure 7: The orientational order parameter profile $\eta_{10}(z) = <\cos\theta>$ of a dipole component of electrolyte solution near a charged hard wall. The ionic concentration $c = 10\,mM$, the dipole moment strength $m^* = 2.4$. The results are compared with the corresponding ones for pure dipole fluid (the curve $c = 0$). a). The wall electric potential $\varphi_0 = 6.4\,mV$ (the corresponding wall charge density $\sigma = 1.48 \cdot 10^{-4}\,\frac{C}{m^2}$); \quad b). $\varphi_0 = 25.7\,mV$ ($\sigma = 6.26 \cdot 10^{-3}\,\frac{C}{m^2}$).
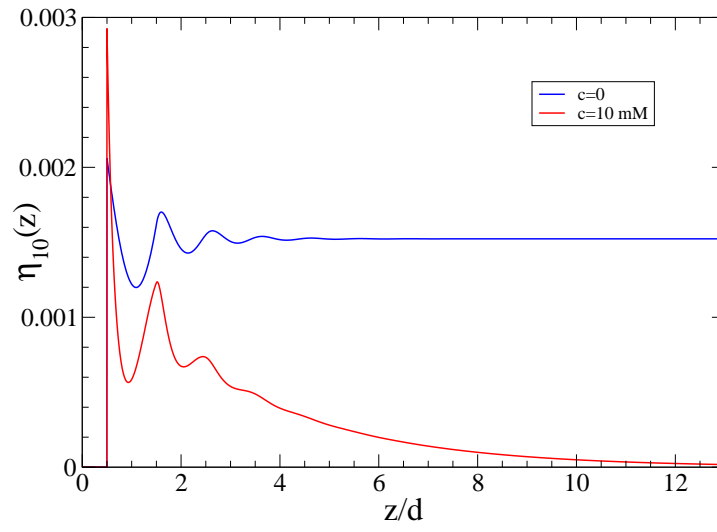
a)
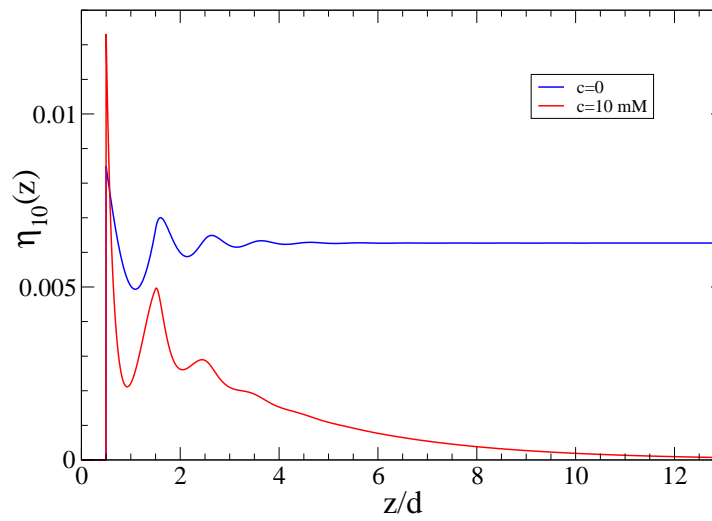
b)

Figure 8: The same as in Fig.7, but for the dipole moment strength $m = 0.93\,D$. a).$\varphi_0 = 6.4\,mV$ $(\sigma = 3.80 \cdot 10^{-4}\,\frac{C}{m^2})$;   b). $\varphi_0 = 25.7\,mV$ $(\sigma = 1.57 \cdot 10^{-3}\,\frac{C}{m^2}$
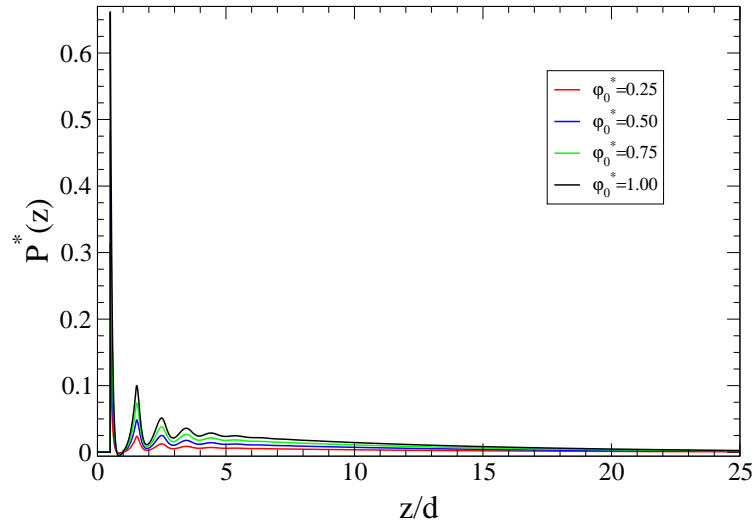
Figure 9: The dimensionless polarization profiles $P^*(z)$ for different values of the wall electric potential φ_0^*. The values of the parameters of PSCDFT are the same as the ones in Fig.4.
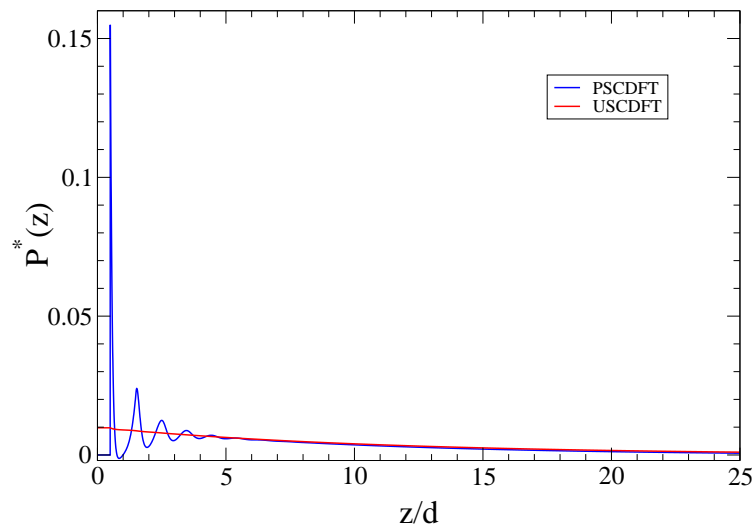

Figure 10: The dimensionless polarization profiles $P^*(z)$ for the wall electric potential $\varphi_0^* = 0.25$. The result for PSCDFT is compared to the corresponding one for USCDFT. The values of parameters are the same as the ones in Fig.4.
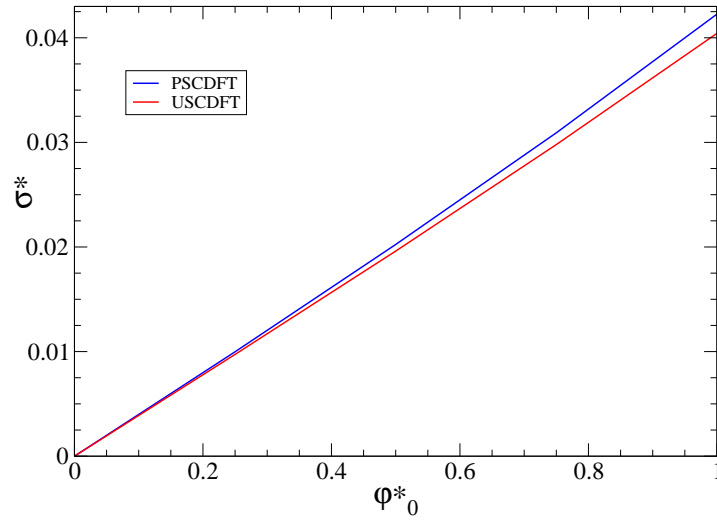
Figure 11: The dependence of a wall charge density σ^* on the wall electric potential φ_0^*. The results for PSCDFT are compared with the ones for USCDFT. The values of parameters are the same as the ones in Fig.4.
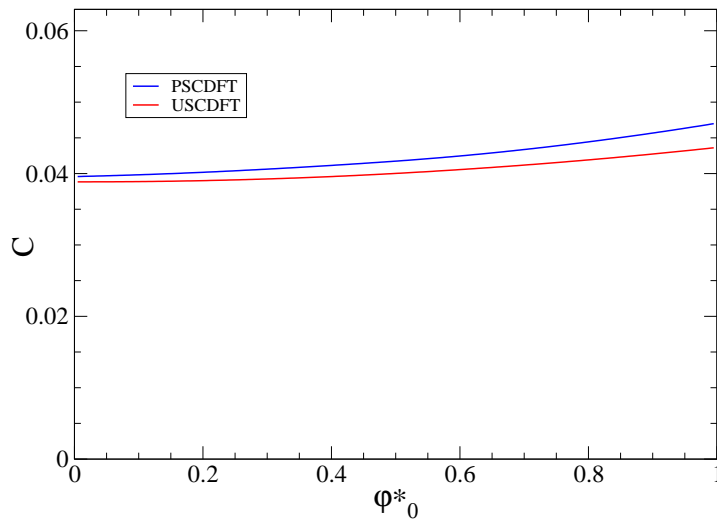

Figure 12: The same as in Fig. 11, but for the differential capacitance $C = d\sigma^*/d\varphi_0^*$.
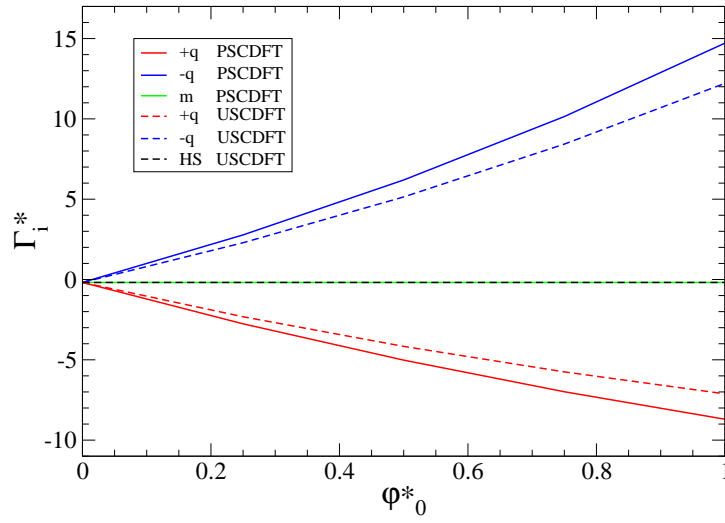
Figure 13: The scaled excess adsorptions Γ_i^* ($i = 1, 2, 3$) as functions of the wall electric potential φ_0^*. The results for PSCDFT are compared with the ones for USCDFT. The notations and the values of the parameters of the electrolyte solution are the same as the ones in Fig.4.
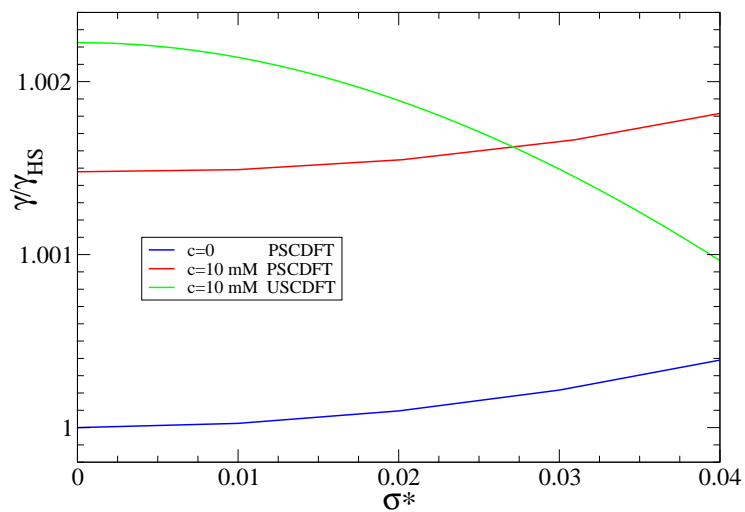
Figure 14: The scaled wall-fluid surface tension γ/γ_{HS} as a function of the wall charge density σ^*. The result for PSCDFT are compared with the corresponding one for USCDFT. The values of parameters are the same as the ones in Fig.4.
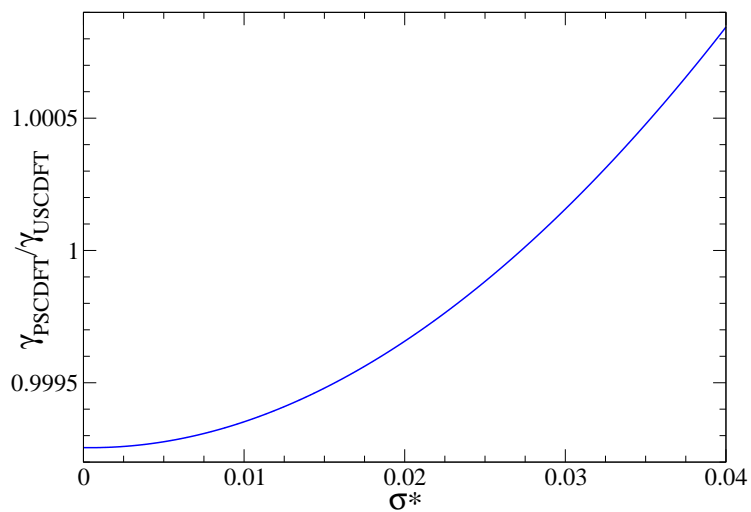

Figure 15: The ratio of wall-fluid PSCDFT surface tension γ_{PSCDFT} and USCDFT surface tension γ_{USCDFT} as a function of the wall charge density σ^*. The values of parameters are the same as the ones in Fig.4.